

ORIGINAL PAPER

Open Access



Subduction of a rifted passive continental margin: the Pohorje case of Eastern Alps—constraints from geochronology and geochemistry

Ruihong Chang¹ , Franz Neubauer^{1*} , Yongjiang Liu^{2,3} , Johann Genser¹ , Wei Jin⁵, Sihua Yuan⁴, Qingbin Guan², Qianwen Huang² and Weimin Li⁵

Abstract

This study presents geochronological and geochemical data from newly dated Permian granitic orthogneisses associated with the Eclogite-Gneiss unit (EGU) from the southernmost part of the Austroalpine nappe stack, exposed within the Pohorje Mountains (Slovenia). LA-ICP-MS zircon U–Pb ages of two samples of the augen-gneisses are 255 ± 2.2 Ma and 260 ± 0.81 Ma, which are interpreted as the age of magmatic crystallization of zircon. In contrast, all round zircons from leucogneisses give Cretaceous ages (89.3 ± 0.7 Ma and 90.8 ± 1.2 Ma), considered as the age of UHP/HP metamorphism. The round zircons overgrew older euhedral zircons of Permian and rare older ages tentatively indicating that these rocks are of latest Permian age, too. Zircon $\varepsilon_{\text{Hf}}(t)$ values of the four orthogneiss samples are between -13.7 and -1.7 with an initial $^{176}\text{Hf}/^{177}\text{Hf}$ ratio ranging from 0.282201 to 0.282562; T_{DM}^{C} is Proterozoic. The augen-gneisses show geochemical features, e.g. high $(\text{La}/\text{Lu})_{\text{N}}$ ratios and strong negative Eu anomalies, of an evolved granitic magma derived from continental crust. The leucogneisses are more heterogeneously composed and are granitic to granodioritic in composition and associated with eclogites and ultramafic cumulates of oceanic affinity. We argue that the Permian granitic orthogneisses might be derived from partial melting of lower crust in a rift zone. We consider, therefore, that segment of the EGU is part of the distal Late Permian rift zone, which finally led to the opening of the Meliata Ocean during Middle Triassic times. If true, the new data also imply that the Permian stretched continental crust was potentially not much wider than ca. 100 km, was subducted and then rapidly exhumed during early Late Cretaceous times.

1 Introduction

A-type subduction is considered to occur at the initial stage of continent–continent collision after consumption of an intervening oceanic lithosphere and subduction of the stretched passive margin. In many cases, the UHP/HP metamorphic conditions are well known but data on the type of subducted continental crust is lacking. In

terms of end members, the type of subducted continental crust is either (1) normal thick continental crust or (2) the crust of a rift zone later transformed to a passive margin, which is influenced by strong extension, high-temperature metamorphism due to thinning of even the subcontinental mantle lithosphere and intense bimodal magmatism. To resolve these alternative scenarios, we investigated the southernmost part of the Eclogite-Gneiss Unit (EGU) and associated units of Cretaceous metamorphic age (Fig. 1a), which is part of the Austroalpine nappe stack and which is exposed in the Pohorje Mountains in the southeasternmost part of the Eastern Alps (Fig. 1b).

Editorial Handling: Othmar Müntener

*Correspondence: Franz.Neubauer@sbg.ac.at

¹ Department of Geography and Geology, University of Salzburg, 5020 Salzburg, Austria

Full list of author information is available at the end of the article



© The Author(s) 2020. This article is licensed under a Creative Commons Attribution 4.0 International License, which permits use, sharing, adaptation, distribution and reproduction in any medium or format, as long as you give appropriate credit to the original author(s) and the source, provide a link to the Creative Commons licence, and indicate if changes were made. The images or other third party material in this article are included in the article's Creative Commons licence, unless indicated otherwise in a credit line to the material. If material is not included in the article's Creative Commons licence and your intended use is not permitted by statutory regulation or exceeds the permitted use, you will need to obtain permission directly from the copyright holder. To view a copy of this licence, visit <http://creativecommons.org/licenses/by/4.0/>.

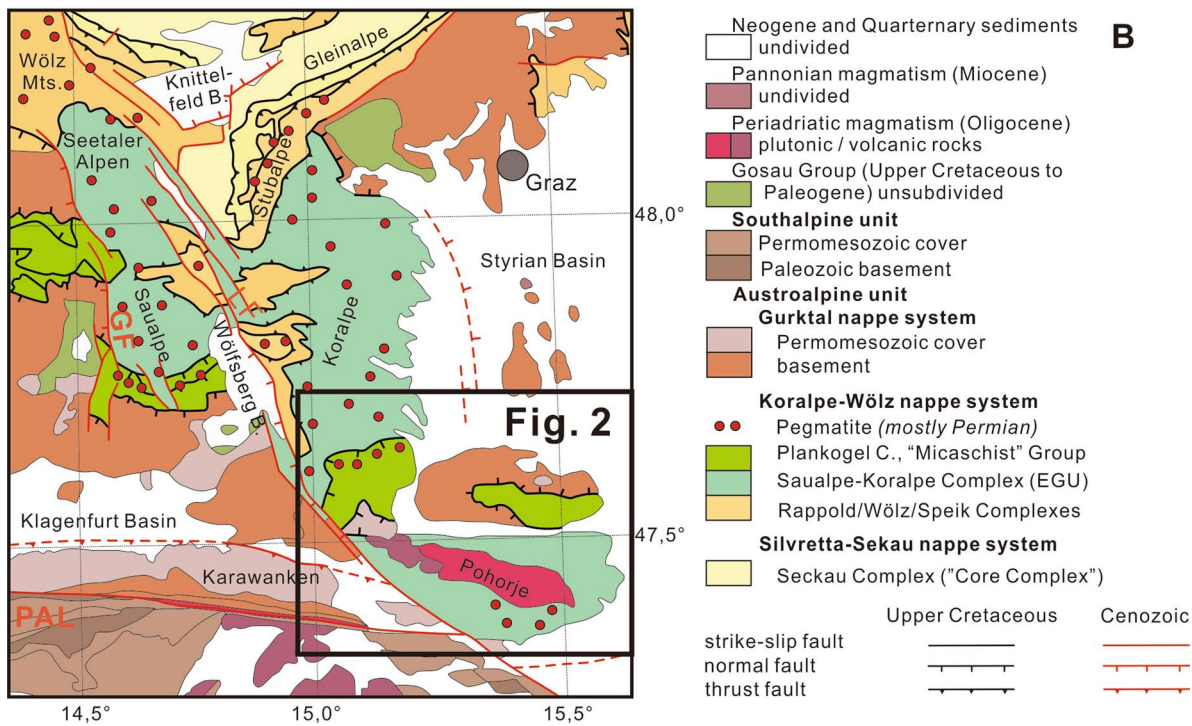
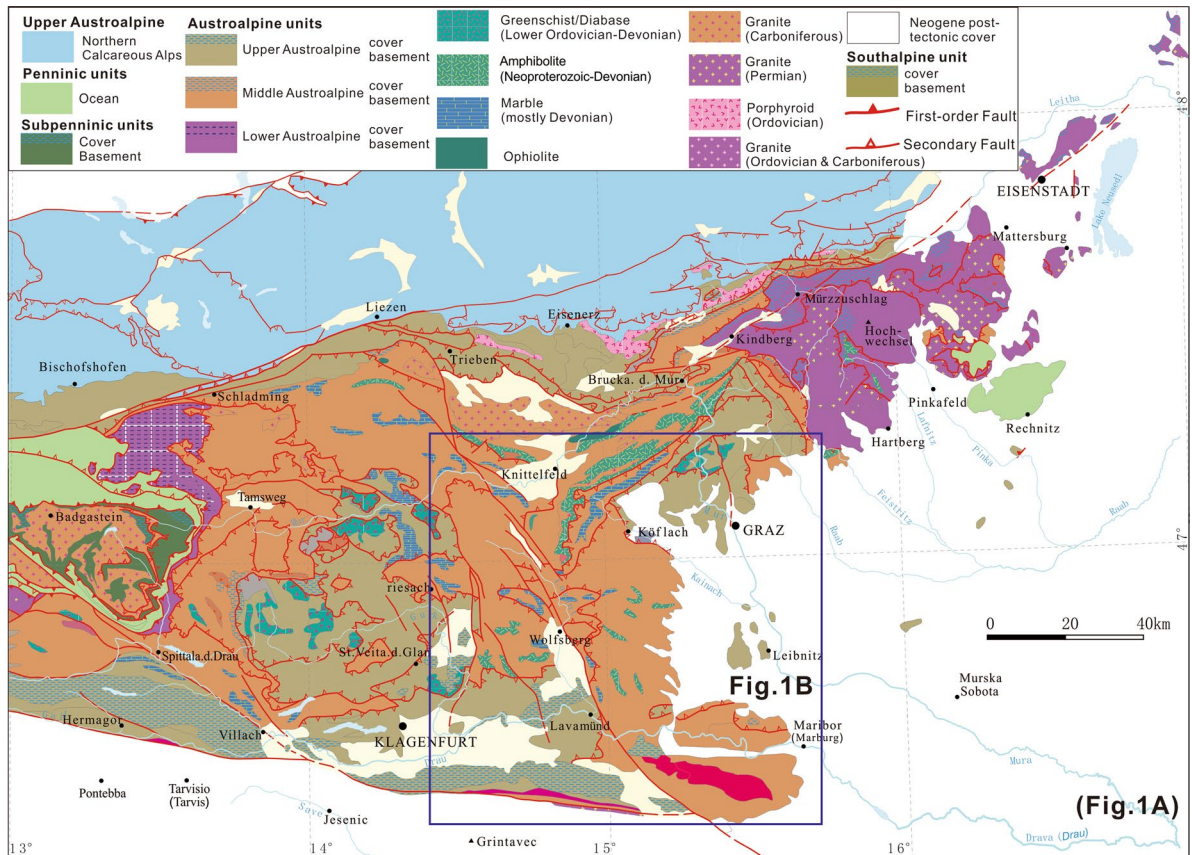


Fig. 1 a Geological map of the eastern part of the Eastern Alps. **b** Tectonic map of the Saualpe-Koralpe-Pohorje area (modified after Miller et al. 2005a)

There, UHP eclogites and ultramafic mantle rocks are exposed in a matrix of paragneiss and associated with hitherto undated granitic orthogneisses (Kirst et al. 2010; Janák et al. 2015).

The Alps are the type continent–continent collisional orogenic belt (Schmid et al. 2004). The Eastern Alps in particular, are the result of the convergence of two independent Alpidic collisional orogenic belts (Neubauer et al. 2000; Froitzheim et al. 2008). The main tectonic events of the Austroalpine nappe stack, which stretches from the Eastern Alps to the Western Carpathians, are (1) rifting and lithospheric thinning in the Permian following the Variscan orogeny and deposition of Late Carboniferous Variscan molasse; (2) Middle Triassic opening of the oceanic Meliata basin; (3) Jurassic convergence and subduction of the Meliata basin; (4) internal nappe stacking within the Austroalpine nappe complex after closure of the Meliata oceanic basin during Early Cretaceous times; and (5) Paleogene collision of the southern margin of the stable European continent and the Austroalpine nappe complex after the subduction of the South Penninic ocean under the Austroalpine microplate (Neubauer et al. 2000; Schuster et al. 2008; Froitzheim et al. 2008; Thöni et al. 2008; Janák et al. 2004, 2006, 2009; Sassi et al. 2004; Miller et al. 2005a, 2005b, 2007; Bruand et al. 2010; Kirst et al. 2010).

This paper presents the first evidence for Permian granites within or associated with EGU exposed in the Pohorje Mountains of Slovenia. We describe here the petrography, whole-rock geochemistry, zircon U–Pb and Hf isotopic data of four samples, which represent two distinct groups of orthogneisses. We use these data to constrain the petrogenesis of the two types of orthogneisses and their tectonic setting. Integrating collected data with results of previous studies of eclogite, gabbro and ultramafic rocks, we discuss the significance of Permian magmatic and tectonic events, interpret these as rifting followed by Middle-Late Triassic passive margin formation and discuss then the subduction processes of this rifted passive continental margin.

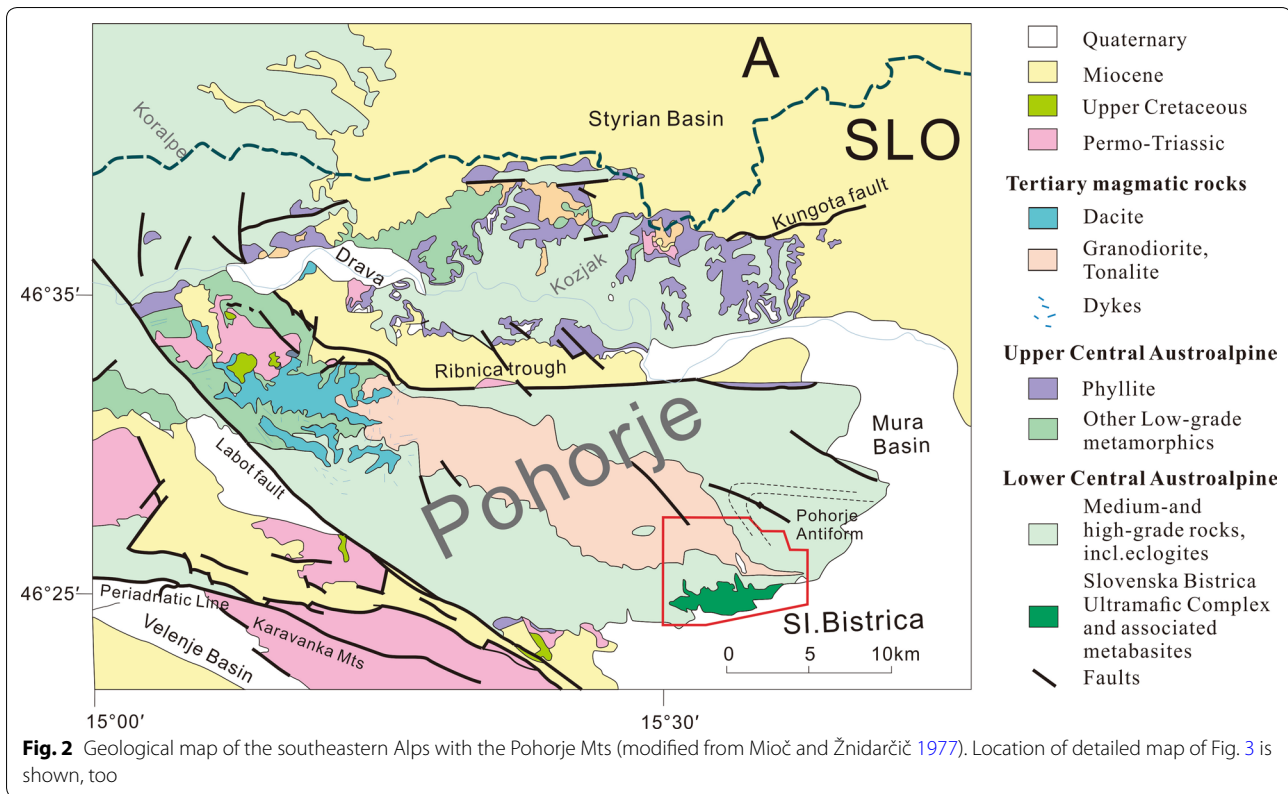
2 Geological setting

The Pohorje Mountains in NE Slovenia are located at the southeastern part of the Eastern Alps just north of the Periadriatic Line (Fig. 1). Together with the Saualpe and Koralpe areas exposed in the north and some small remnants in the Siegraben at the eastern termination of Eastern Alps, the Pohorje Mts. belong to the above mentioned Eclogite-Gneiss unit, recently considered as a part of the Koralpe-Wölz nappe system, which is part of the Lower Central Austroalpine units with respect to the Eo-Alpine UHP/HP subduction zone (Janák et al. 2004; Kirst et al. 2010; Sandmann et al. 2016; Fig. 2) and was

labeled as Middle Austroalpine in the previous literature (e.g., Neubauer et al. 2000). EGU comprises a succession of metamorphic rocks with continental affinity and includes various paragneisses, rare marble and quartzites and intercalated eclogites, rare metagabbro and pegmatites (e.g. Miller et al. 2005a, 2005b). At its southernmost exposures, this succession is in direct contact with a km-sized ultramafic body termed as Slovenska Bistrica Ultramafic Complex (Kirst et al. 2010) (Fig. 3). Based on widespread andalusite paramorphs in paragneisses, EGU is affected by Permian low-pressure metamorphism, whereas the presence of Variscan metamorphism is uncertain. During early Late Cretaceous, these rocks were subducted towards the SE beneath the units of the Upper Central Austroalpine. The subduction polarity is indicated by a south-eastward increase in peak pressures along the Koralpe/Pohorje traverse (Janák et al. 2004; Bruand et al. 2010; Sandmann et al. 2016).

In the Pohorje Mts., the uppermost nappe is the south-eastern extension of the Gurktal nappe system and comprises low-grade metamorphic Paleozoic metasediments overlain by non-metamorphic Permo-Triassic sedimentary rocks (Fig. 2). The metamorphic series of the underlying Eclogite-Gneiss unit (here locally termed Pohorje nappe) mainly comprises gneisses and schists with minor marbles and quartzites and embedded bodies and lenses of eclogite and amphibolite and few orthogneisses and augen gneisses (Janák et al. 2004; Sandmann et al. 2016). At the south-eastern margin of the Pohorje Mts., the Slovenska Bistrica Ultramafic Complex (SBUC) extends over 8 km in E–W direction. This body consists of serpentized ultramafites, eclogites and amphibolites as well as minor garnet-bearing ultramafic rocks (Sassi et al. 2004; Janák et al. 2006; Kirst et al. 2010; De Hoog et al. 2009, 2011). The Pohorje Mts. are intruded by the Miocene Pohorje granodiorite to tonalite (Fodor et al. 2008).

Two stages of metamorphism affected the EGU. The dominant HP–UHP metamorphism is preceded by a HT–LP metamorphic event, expressed by andalusite pseudomorphs. It is interpreted as Permian rifting event (Schuster and Stüwe 2008) causing metamorphism of Paleozoic and older sediments of continental and oceanic affinity. Rifting also led to underplating and emplacement of gabbros in the Koralpe region into the thinned continental crust (Thöni and Jagoutz 1992; Thöni et al. 2008). Sm–Nd ages of these metagabbros are 275 ± 18 Ma for protolith crystallization and 93 ± 15 Ma for eclogite metamorphism (Thöni and Jagoutz 1992). Furthermore, numerous seemingly rootless pegmatite bodies of Permian age are preserved in the EGU and in underlying and overlying units (Knoll et al. 2018 and references therein; Fig. 1b).



The timing of UHP/HP metamorphism in the Pohorje Mts. is generally accepted to be Eo-Alpine (i.e. Cretaceous). U–Pb zircon ages of eclogites and metapelites are c. 93–90 Ma, (Janák et al. 2009; Miller et al. 2005b). Sm–Nd garnet ages of eclogites from the Saualpe, Koralpe and Pohorje areas are in the range of 108 to 87 Ma (Thöni 2002). K–Ar and Ar–Ar muscovite ages are 85–90 Ma in the northern part of the nappe system (as well as in the underlying Gleinalpe-Stubalpe region; Neubauer et al. 1995) and about 75–80 Ma in the central part (Saualpe-Koralpe region) (Miller et al. 2005b; Wiesinger et al. 2006; Thöni et al. 2008), Lu–Hf ages for Grt–Omp and Grt–Cpx of eclogites and ultramafic rocks, respectively, from the Pohorje EGU are between 97 and 92 Ma (Sandmann et al. 2016). These geochronological data indicate a maximum burial of the Eclogite-Gneiss unit in the Cenomanian and Turonian (Thöni et al. 2008), followed by rapid exhumation in the Coniacian and Santonian (Wiesinger et al. 2006). Wiesinger et al. (2006) documented a N-directed thrust fault at the base of EGU, whereas the upper contact is a ductile low-angle normal fault (Ratschbacher et al. 1989; Wiesinger et al. 2006), later called Plankogel detachment (Schorn and Stüwe 2016). Neogene fault systems have a major influence on the recent morphology and are responsible for the final exhumation of the Saualpe-Koralpe Complex in the Pohorje region

(Ratschbacher et al. 1989, 1991). The Miocene Pohorje granodiorite reveals that the region was still buried during Early Miocene, whereas in the surrounding Pannonian basin sediment deposition was already ongoing (Fodor et al. 2008).

3 Samples and petrography

In this study, we focus on two augengneiss, and two leucogneiss samples. All rocks are deformed and metamorphic granitic gneisses, but show quite different characteristics. The augengneisses are Bt-gneisses which still show some magmatic features, the leucogneiss samples are Grt–Ms-gneisses. The protolith of the augengneisses intruded a sequence of gneisses with intercalations of micaschists, amphibolite and marbles (Kirst et al. 2010), the leucogneiss samples are associated with eclogites, Bt-gneisses and UHP-paragneisses and micaschists (Janák et al. 2015).

The two augengneiss samples (SK1, SK2) were collected from an orthogneiss body, located ~0.5 km to southwest of Zgornje Prebukovje (Fig. 3, Table 1). This type of orthogneiss is dominated by augengneiss, which is characterized by large ovoidal megacrysts of feldspar (mainly K-feldspar) (25%) (Fig. 4a) within fine-grained granitic mineral assemblages (Fig. 4b). The matrix mainly comprises fine-grained plagioclase (25–30%), K-feldspar

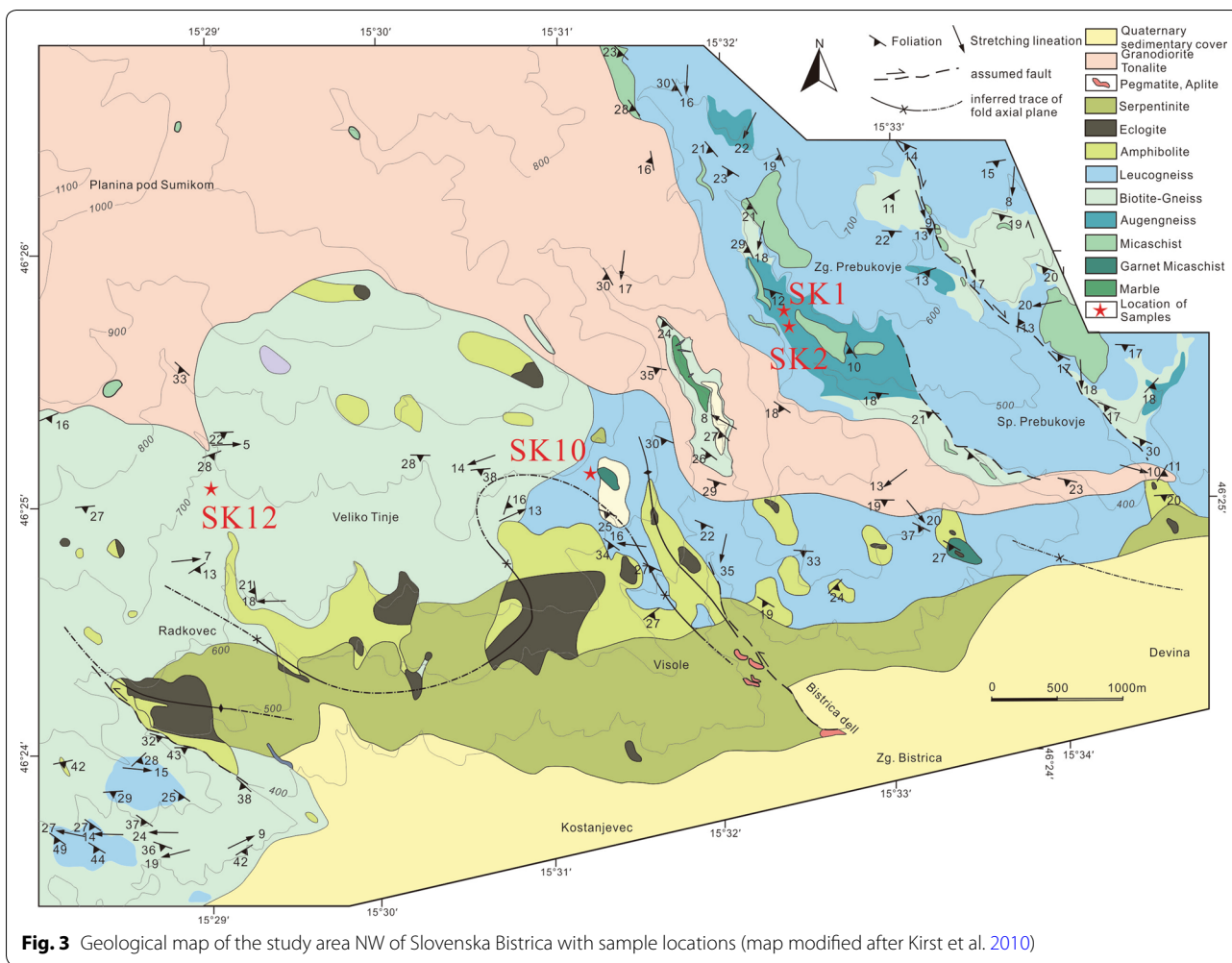
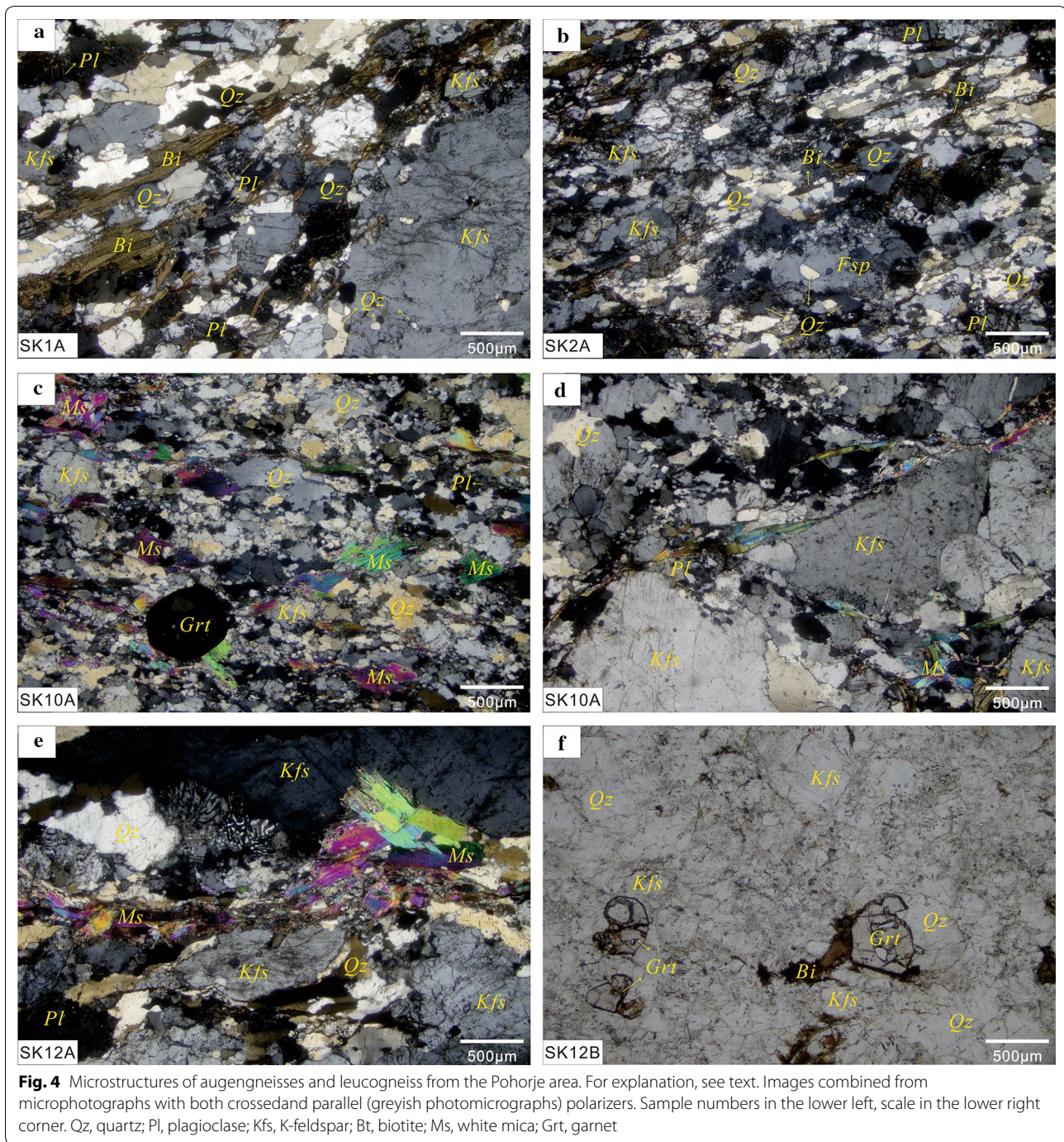


Fig. 3 Geological map of the study area NW of Slovenska Bistrica with sample locations (map modified after Kirst et al. 2010)

Table 1 Petrography and structural characteristics of samples

Sample no.	Coordinates WGS-84	Lithology	Mineral assemblage	Microscopic structures	DT (°C)
SK1	N 46°25.8' E 15°32.4'	Augengneiss	Augen (25%): Kfs + Qtz; 1–1.5 mm. Matrix(75%): Qtz + Pl + Kfs + Bi; Ms < 2% with a size of 0.05–0.5 mm	Qtz: fine-grained, undulatory extinction, deformation bands, BLG, SGR; Kfs: BLG, deformation twins; Pl: micro-fractures; Bi: oriented. Stretching lineation, augen structure.	± 500
SK2	N 46°25.7' E 15°32.4'	Augengneiss	Augen (20%): Kfs + Qtz; 0.5–1 mm. Matrix(80%): Qtz + Pl + Kfs + Bi; Ms < 2%, grain-size: 0.05–0.5 mm	Qtz: monocrystals elongated, partly undulatory extinction; Fsp: elongated, BLG; Pl: deformation twins; Bi: oriented. Stretching lineation, augen structure.	± 500
SK10	N 46°25.1' E 15°31.3'	Leucogneiss	Qtz: 25%; Pl: 25%; Kfs: 30%; Ms: 8%; Grt: 5%.	Qtz: fine-grained, SGR; Kfs: micro-fractures Pl: albite twins; Ms: oriented; garnet: core-rim structure	± 600
SK12	N 46°25.1' E 15°29.0'	Leucogneiss	Qtz: 30%; Pl: 20%; Kfs: 25%; Ms: 10%; Grt: 3%; Bi: < 3%	Qtz: fine grained, weakly elongated, SGR, GBM; Kfs: micro-fractures; myrmekitic texture in Kfs grains	± 600

Qtz: quartz; Fsp, feldspar; Pl, plagioclase; Afs, alkali feldspar; Bi, biotite; Ms, muscovite; BLG, bulging; SGR, subgrain rotation; GBM (grain boundary migration); DT, deformation temperature, which is estimated based on Stipp et al. (2002a, 2002b, 2010)



(30–40%), quartz (30–35%), biotite (10–15%), which is sometimes retrogressed to chlorite, muscovite (<2%), and a small number of accessory minerals (magnetite, apatite, zircon, ilmenite) and has an allotriomorphic granular texture (Fig. 4a). Quartz grains in the augengneiss are generally elongated and the light bands composed of quartz and feldspar alternate with thin stripes of biotite (Fig. 4b).

The two leucogneiss samples (SK10 and SK12) were collected ~1 km east and 1.5 km west of Veliko Tinje village, respectively (Fig. 3, Table 1). According to the map of Kirst et al. (2010) sample SK10 is from a leucogneiss body, sample SK12 from a biotite-gneiss unit. Both leucogneiss samples consist of quartz, plagioclase, K-feldspar, white mica, garnet, and some late-stage biotite (Fig. 4c, d, e, f). Zircon, apatite, and magnetite occur as

minor constituents. Simple inclusion-free garnet porphyroblasts are common (Fig. 4c, f). Large K-feldspar phenocryst show graphic intergrowths with quartz. Myrmekites are often developed in K-feldspar in contact with plagioclase (Fig. 4d, e). Quartz grains with an average size from 0.1 to 0.8 mm indicate dynamic recrystallization by sub-grain rotation and grain boundary migration (Fig. 4g).

4 Analytical methods

4.1 Zircon U–Pb dating

Zircons from the four representative orthogneiss samples (SK1, SK2, SK10, SK12) (Fig. 3) were dated by the U–Pb method.

Zircon grains were extracted from samples using conventional density and magnetic separation techniques at the Yuneng Mineral Separation Company, Hebei Province. Over 500 zircons were handpicked under a binocular microscope, then mounted in epoxy resin and polished until the grain centers were exposed. To remove any lead contamination, the surface was cleaned using 3% HNO₃ prior to analysis. Cathodoluminescence (CL) images were obtained using a Mono CL3+ microprobe, in order to characterize internal structures and to choose potential target sites for U–Pb dating.

Measurements of U, Th, and Pb isotope data and trace element compositions were conducted using a high-precision laser ablation-inductively coupled plasma–mass spectrometer (LA-MC-ICP-MS) at the Beijing Createch Testing Technology Co., Ltd. Detailed operating conditions for the laser ablation system and the MC-ICP-MS instrument and data reduction are the same as described by Hou et al. (2009). Laser sampling was performed using a Resolution 193 nm laser ablation system. A 24 μm spot size was adopted in this study with a laser repetition rate of 6 Hz and energy density up to 6 J/cm². Helium was applied as a carrier gas from the sample chamber to the analyzer. An Agilent 7500 ICP-MS instrument was used to acquire ion-signal intensities. Each analysis incorporated background acquisition of approximately 15–20 s (gas blank) followed by 45 s data acquisition from the sample. Off-line raw data selection and integration of background and analytical signals, and time-drift correction and quantitative calibration for U–Pb dating was performed by ICPMSDataCal (Liu et al. 2010).

Zircon GJ-1 (Jackson et al. 2004) was used as external standard for U–Pb dating, and was analyzed twice every 5–10 analyses. Time-dependent drifts of U–Th–Pb isotopic ratios were corrected using a linear interpolation (with time) for every 5–10 analyses according to the variations of GJ-1 (i.e., 2 zircon GJ-1 + 5–10 samples + 2 zircon GJ-1) (Liu et al. 2010). Uncertainty of preferred values for the external standard GJ-1 (with an age of

599.6 ± 2.9 Ma) was propagated to the ultimate results of the samples. No common Pb correction was necessary due to the low signal of common ²⁰⁴Pb and high ²⁰⁶Pb/²⁰⁴Pb ratios. U, Th and Pb concentrations were calibrated by NIST 610. Concordia diagrams and weighted mean calculations were made using Isoplot/Ex_ver3 (Ludwig 2003).

4.2 Zircon Hf isotope analysis

In situ zircon Hf isotope analyses were performed on the same zircon grains that were subjected to U–Pb dating at the Beijing Createch Testing Technology Co. Ltd., China, using a Resolution SE 193 nm laser-ablation system attached to a Thermo Fisher Scientific Neptune Plus ICP. Instrumental conditions and data acquisition protocols were described by Hou et al. (2007). A stationary spot with a beam diameter of ~38 μm was used for ablation. As carrier gas helium was used to transport the ablated sample aerosol mixed with argon from the laser-ablation cell to the MC-ICP-MS torch. ¹⁷⁶Lu/¹⁷⁵Lu = 0.02658 and ¹⁷⁶Yb/¹⁷³Yb = 0.796218 ratios were applied to correct for the isobaric interferences of ¹⁷⁶Lu and ¹⁷⁶Yb on ¹⁷⁶Hf. For instrumental mass bias correction Yb isotope ratios were normalized to ¹⁷²Yb/¹⁷³Yb = 1.35274 and Hf isotope ratios to ¹⁷⁹Hf/¹⁷⁷Hf = 0.7325 using an exponential law. The mass bias behavior of Lu was assumed to follow that of Yb, the mass bias correction protocol was described by Hou et al. (2007). Further external adjustment was not applied to the unknowns because our determined ¹⁷⁶Hf/¹⁷⁷Hf ratios of 0.282004 ± 38 (2SD, n = 107) for zircon standard GJ-1 are in good agreement with the reported values (0.282000 ± 0.000005) (Morel et al. 2008). Hafnium isotopic data are age-corrected using the ¹⁷⁶Lu decay constant of 1.867 × 10⁻¹¹ a⁻¹ (Soderlund et al. 2004). εHf(t) values and Hf model ages were calculated using the methods of Bouvier et al. (2008) and Griffin et al. (2002), respectively.

4.3 Whole-rock major and trace element determinations

In addition to the four dated samples, we collected in each outcrop several additional samples for geochemical analysis. These are similar in petrography varying slightly in the amount of main minerals and microfabrics. The major and trace element compositions of 13 multiple samples from the four magmatic rocks from the studied area were determined by X-ray fluorescence (XRF-1800; Shimadzu) on fused glasses and inductively coupled plasma mass spectrometry (Agilent 7500ce ICP-MS) at Beijing Createch Test Technology Co. Ltd. Prior to analysis, all samples were trimmed to remove weathered surfaces before being cleaned with deionized water and crushed to 200 mesh in an agate mill. Sample powders (~40 mg) were digested using HNO₃ and HF acids in

Teflon bombs. Loss-of-ignition (LOI) values were measured after heating 1 g of sample in a furnace at 1000 °C for several hours in a muffle furnace. The precision of the XRF analyses is within $\pm 2\%$ for the oxides greater than 0.5 wt% and within $\pm 5\%$ for the oxides greater than 0.1 wt%.

Sample powders (about 50 mg) were dissolved in Teflon bombs using a HF + HNO₃ mixture for 48 h at about 190 °C. The solution was evaporated to incipient dryness, dissolved by concentrated HNO₃ and evaporated at 150 °C to dispel the fluorides. The samples were diluted to about 100 g for analysis after redissolving in 30% HNO₃ overnight. An internal standard solution containing the element Rh was used to monitor signal drift during analysis. Analytical results for USGS standards for ICP-MS (Jochum et al. 2005) indicate that the accuracy for most elements were within 5%.

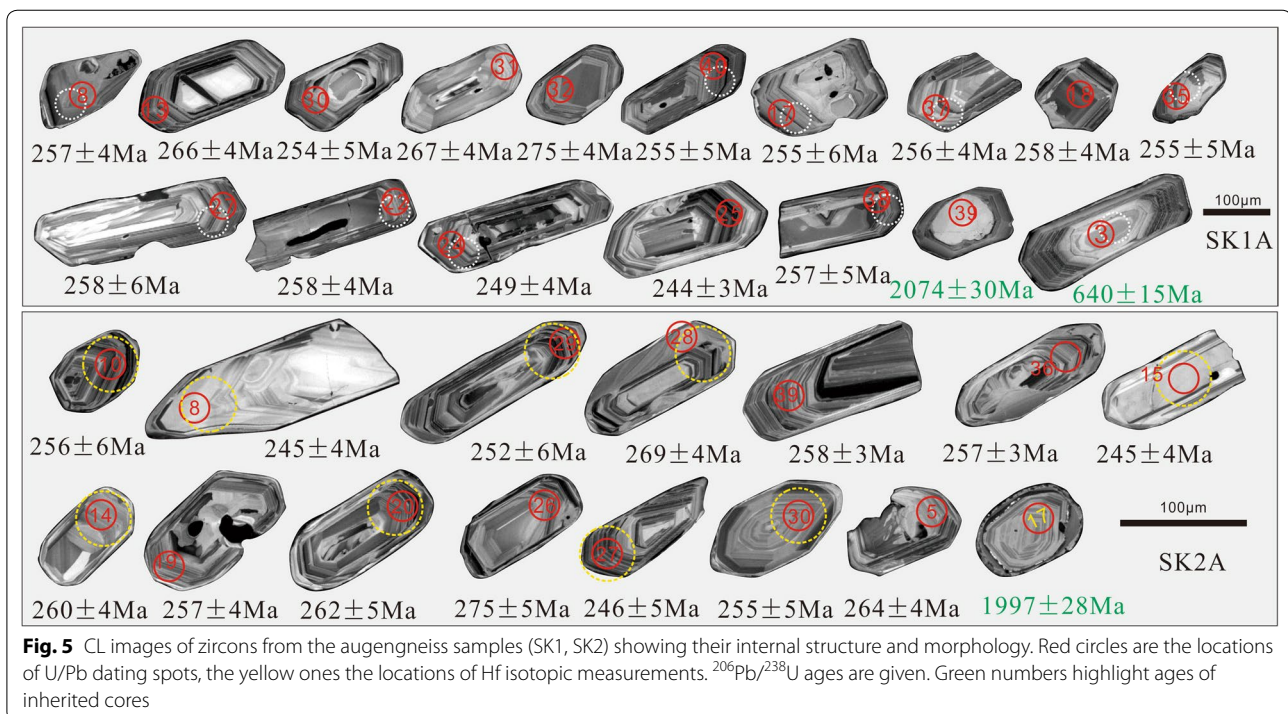
5 Results

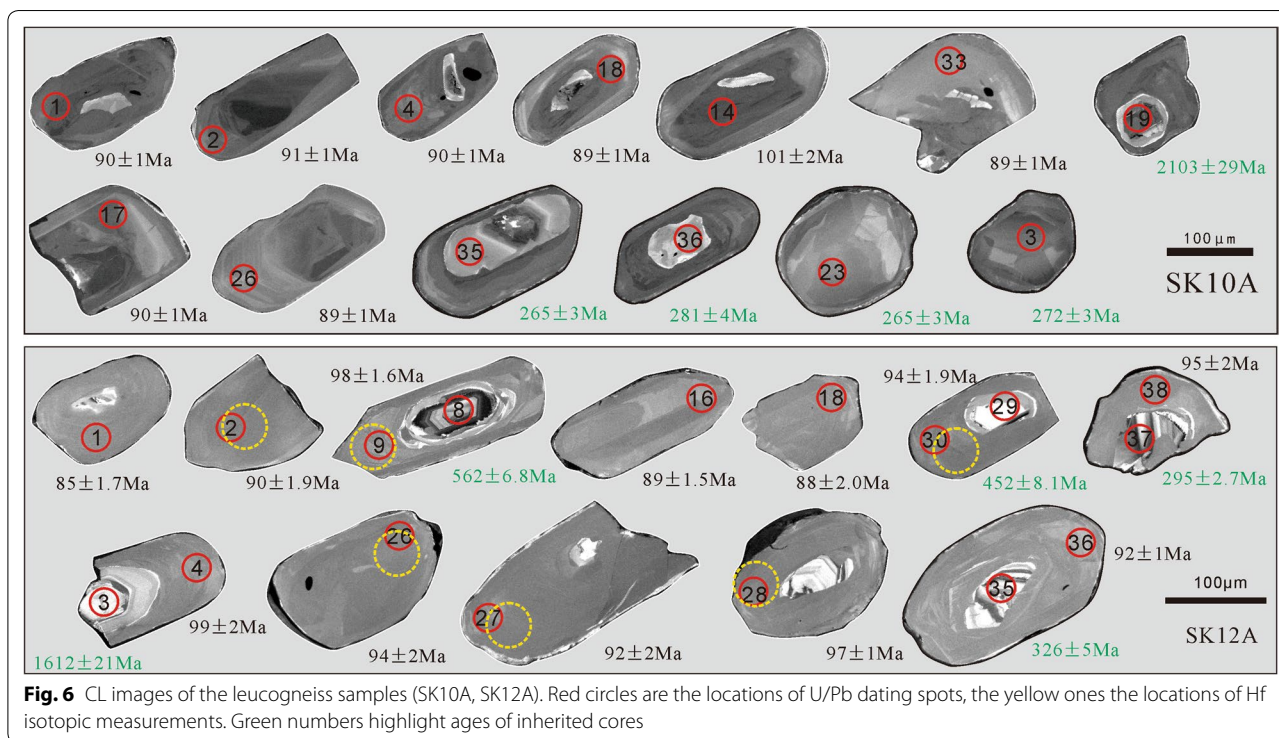
5.1 U–Pb zircon dating

Zircons in CL images show that igneous zircons with oscillatory zoning in Fig. 5 but metamorphic ones with relic cores in Fig. 6. The zircon U–Pb isotopic data are given in Additional file 1: Table S1 and are graphically shown in Figs. 7 and 8. The ages given in the text are concordia ages except for the few inherited ages of more than 1000 Ma, for which the ²⁰⁶Pb/²³⁸Pb ages are given.

The zircon grains of the two augengneiss samples SK1 and SK2 are mostly subhedral-euhedral, generally

elongated and prismatic and range in length from 100 to 250 μm and in width from 60–100 μm. Most zircon grains exhibit a well-developed oscillatory zoning in CL images (Fig. 5); only a minority of grains contain inherited cores. These characteristics, along with their 67–3631 ppm U and 98–641 ppm Th contents resulting in relatively high Th/U ratios of 0.12–1.30 (except for two zircon rims with 0.08–0.09; Additional file 1: Table S1, Fig. 9a), are typical of magmatic zircons (Hoskin and Schaltegger 2003; Corfu et al. 2003). The chondrite-normalized REE patterns of these zircon grains were dated by the same analytical techniques with U–Pb age on the same spot. Results are given in Additional file 2: Table S2 and are graphically shown in Fig. 9a, reveal a strong depletion in light REEs relative to heavy REEs, and are characterized by strongly negative Eu anomalies, which indicate the presence of plagioclase during the zircon growth (Hoskin and Schaltegger 2003; Rubatto, 2002; 2017). Moreover, relatively steep HREE patterns suggest absence of garnet and low-pressure conditions during the formation of these old zircon domains (Janák et al. 2009) while positive Ce anomalies and negative Eu anomalies are nearly ubiquitous in crustal magmatic zircon (Fig. 9b), Lu/Tb ratios are higher than 5 and up to 10 (Fig. 9a). These geochemical characteristics further support an igneous origin for these zircons (Grimes et al. 2007). Twenty-seven of the 30 analyses of magmatic grains of sample SK1 yield a concordant age of 260.5 ± 0.81 Ma (MSWD of concordance = 4.7; Fig. 7), twenty-nine from thirty analyses of

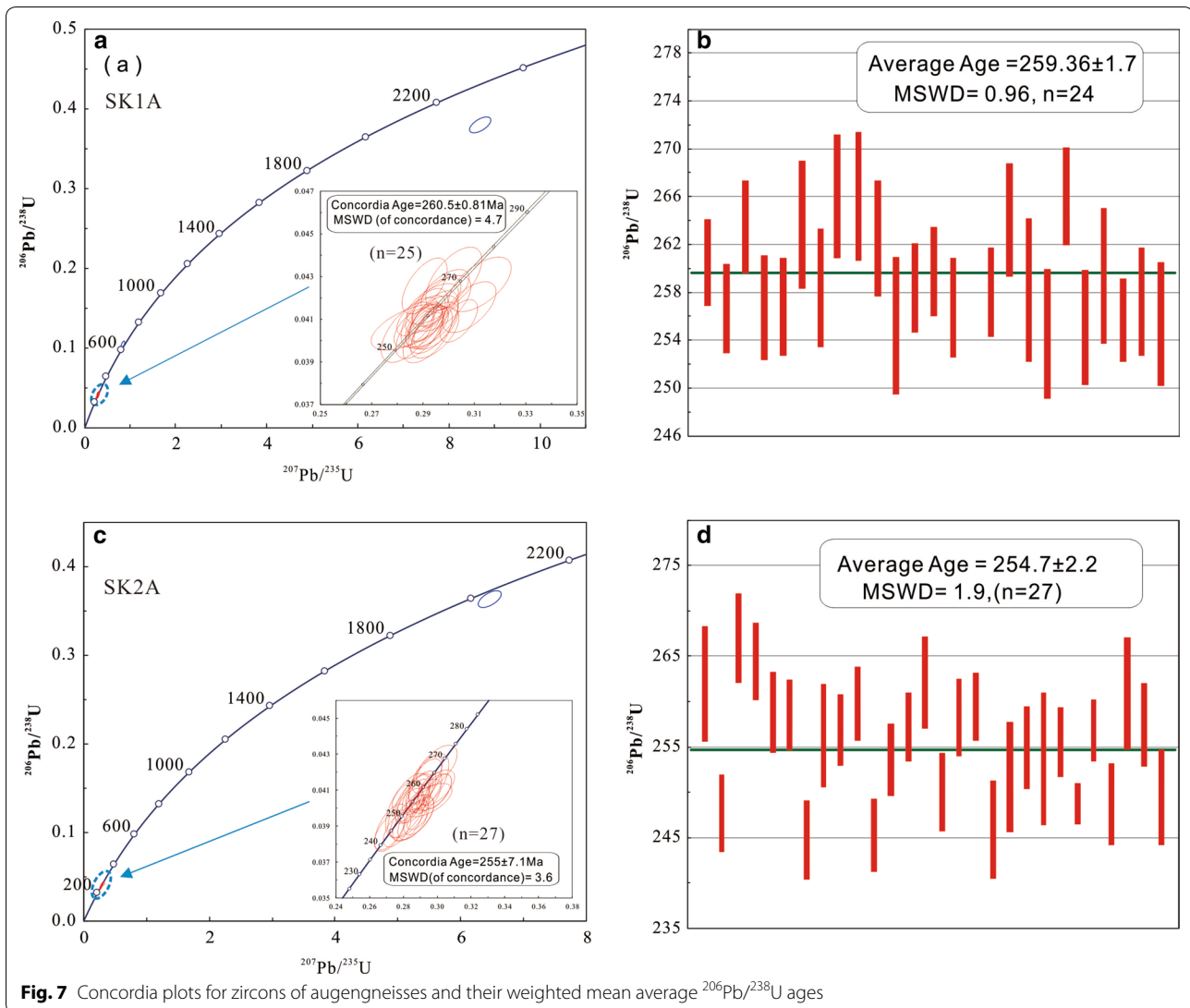




magmatic grains in sample SK2 yield a concordia age of 255 ± 7.1 Ma (MSWD of concordance = 3.6; Fig. 7). We interpret these age data as the time of zircon crystallization in the magma and thus the formation age of the porphyric granites. A few zircon cores have concordia ages that range from 640 ± 15 Ma to 2074 ± 30.4 (Additional file 1: Table S1).

The zircon grains of the two leucogneisses SK10 and SK12 are rounded with only a slightly discernible oscillatory zoning and Th/U ratios of 0.005 to 0.009, except several higher ratios of distinct cores (Additional file 1: Table S1, Fig. 9a). Some grains, however, have inherited cores, with a more clearly discernible oscillatory zoning. The chondrite-normalized REE patterns of these zircon grains show markedly lower REE contents than zircons from the augengneisses (Fig. 9b). There is a clear distinction between REE patterns of old and young domains in the investigated zircons (Fig. 9). They show a relatively flat HREE pattern compared to the HREE enrichment in magmatic zircon, which indicate that these are of metamorphic origin and formed in the presence of a HREE-bearing phase; garnet is commonly a main host of HREE in medium to high-grade mafic to pelitic metamorphic rocks (Rubatto 2017). The absence of a strong negative Eu anomaly suggests growth of zircons in the absence of plagioclase. There are a few magmatic zircons with Eu anomalies in cores. Except sample SK1, all samples have a pronounced positive Ce anomaly typical for crustal

magmatic zircons (Hoskin and Schaltegger 2003). The Lu/Tb composition of zircon can distinguish between magmatic zircons which show increasing normalized HREE-patterns and metamorphic zircons that grew in equilibrium with garnet which show very flat HREE-distributions. In our samples, the normalized Lu/Tb ratios of metamorphic zircons is generally < 5 , just several cores in zircon show high Lu/Tb ratios. Especially in sample SK10, these zircons reveal the presence of strongly luminescent cores and darker rims consistent with radiation damage suppression of CL in rims with high U contents (Fig. 6). The size of seven zircon cores are large enough to enable U–Pb isotopic dating. The discussion focuses on data obtained from analyzed zircons that record a primary magmatic growth. 31 of 40 analyses of sample SK10 are concordant and 17 of them yield a concordant weighted mean average $^{206}\text{Pb}/^{238}\text{U}$ age of 89.6 ± 0.6 Ma (MSWD of concordance = 0.71) (Fig. 8). Inherited cores of zircon grains have ages ranging between 255 ± 6 Ma and 281 ± 5 Ma and a mode at about 265 Ma; only one analyzed core is much older at 2103 ± 29 Ma (Fig. 6). In sample SK12, 29 of 40 analyses are concordant and 24 spots yielded a $^{206}\text{Pb}/^{238}\text{U}$ weighted mean age of 90.5 ± 0.5 Ma (MSWD of concordance = 0.0057) (Fig. 8). The ages of zircon cores range between 260 ± 3 Ma and 1489 ± 32 Ma (Additional file 1: Table S1, Fig. 8), but there is no grouping of ages unlike for sample SK10. Only



the single youngest age of 260 Ma fits the age group of samples SK10.

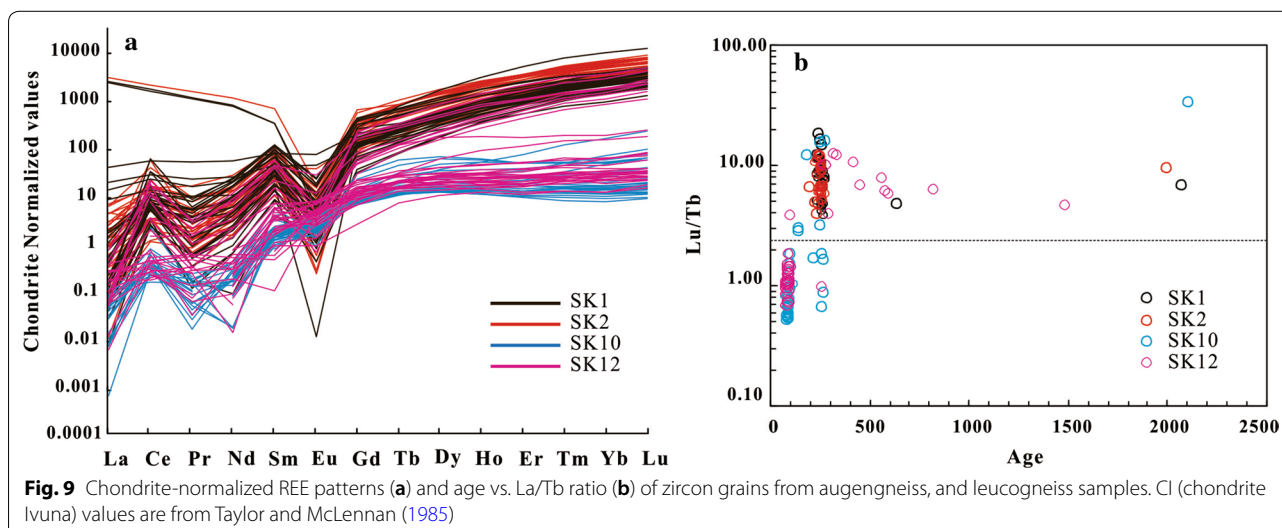
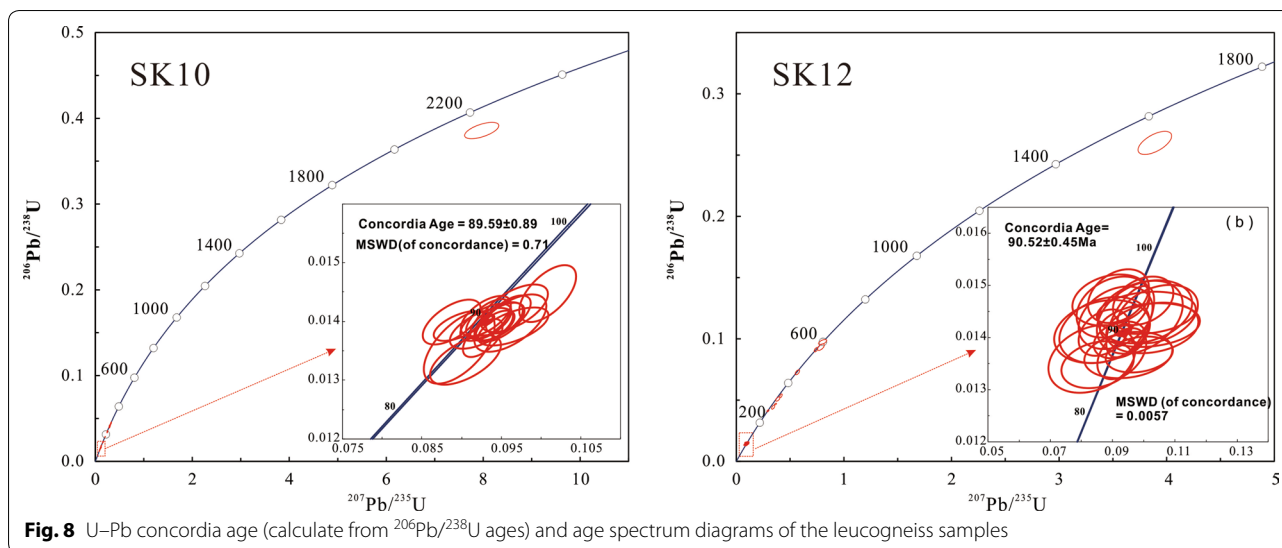
Based on the CL-attributes, the REE contents and patterns, Lu/Tb ratios and the ages the zircons must represent metamorphic growth or recrystallization, thus dating the HP-event. The age group at about 265 Ma from oscillatory zoned zircon cores could be interpreted as magmatic formation ages.

5.2 Crystallization temperatures

We calculated the formation temperatures of the orthogneiss samples from the Pohorje area with the whole-rock zirconium saturation thermometer (Boehnke et al. 2013; Watson and Harrison 1983). The zirconium saturation temperatures can provide an estimate of the initial magma temperatures of granites based on the Zr content

and a correction term for the major element chemistry of the whole rock (Boehnke et al. 2013; King et al. 1997; Miller et al. 2003; Watson and Harrison 1983). The input parameters for the thermometer and the calculated zirconium saturation temperatures of the orthogneiss samples are listed in Additional file 3: Table S3.

Based on the very different Zr contents and M factors and the resulting magmatic crystallization temperatures, the orthogneiss samples can be divided into two types: a low and a high temperature type, consistent with the previous grouping. The augengneisses give lower temperatures of ~500–550 °C, whereas the leucogneisses yield higher formation temperatures of ~700–770 °C. Though the calculated temperatures for the augengneisses are unrealistic, this temperature-based subdivision corresponds to the zircon-based subdivision presented above (Table 2).



5.3 Zircon Hf isotopic data

Thirty-five zircon grains of samples SK1, SK2 and SK12 were analyzed for Hf isotopes (Table 2; Fig. 10). The $^{176}\text{Hf}/^{177}\text{Hf}(t)$ values of 20 analyses of magmatic zircon grains from SK1 and SK2 range between 0.282703 and 0.282868 ($t=255$ Ma), which correspond to $\epsilon\text{Hf}(t)$ values between -6.4 and -1.7 and crustal model ages (T_{DM}^{C}) of 1392 to 1617 Ma (Table 2). An inherited zircon core exhibits an $\epsilon\text{Hf}(t)$ value of -6.6 ($t=640$ Ma, $^{176}\text{Hf}/^{177}\text{Hf}_i=0.282201$), which corresponds to a crustal model ages (T_{DM}^{C}) of 1972 Ma.

Eight analyses of zircons from the leucogneiss sample SK12 gave $^{176}\text{Hf}/^{177}\text{Hf}$ values of 0.282385–0.282562. These analyses correspond to $\epsilon\text{Hf}(t)$ values of -13.7 to -7.9 and yield Hf crustal model ages (T_{DM}^{C}) of

969–1195 Ma. These data suggest a predominantly Proterozoic crustal source for both the augengneisses and the leucogneiss with both orthogneiss groups on the same Hf isotope evolution line.

5.4 Geochemistry

In order to chemically characterize and constrain geodynamic settings of the plutonic rocks we analyzed whole-rock major and trace element data which are listed in Table 3. We can use, with due caution regarding the strong Alpine metamorphic overprint, major elements (e.g., Na_2O , K_2O and MgO) combined with high-field-strength elements (HFSE; e.g., Zr, Hf, Nb, Ta, and Ti), transitional elements (e.g., Ni, Cr, V, and Sc), and rare

Table 2 Hf isotopes data of zircons from the Pohorje samples

Sample No.	Age (Ma)	$^{176}\text{Yb}/^{177}\text{Hf}$	2σ	$^{176}\text{Lu}/^{177}\text{Hf}$	2σ	$^{176}\text{Hf}/^{177}\text{Hf}$	2σ	$^{176}\text{Hf}/^{177}\text{Hf}_i$	$e_{\text{Hf}}(0)$	$e_{\text{Hf}}(t)$	$e_{\text{Hf}}(t')$	2σ	T_{DM} (Ma)	T_{DM}^c (Ma)	$f_{\text{Lu/Hf}}$
SK1A-01	640	0.015386	0.000253	0.000529	0.000008	0.282207	0.000018	0.282201	-20.0	-6.1	-5.5	0.6	1457	1958	-0.98
SK1A-02	257	0.015380	0.000617	0.000546	0.000021	0.282530	0.000013	0.282527	-8.6	-3.0	-2.6	0.5	1011	1473	-0.98
SK1A-03	255	0.028399	0.000151	0.001017	0.000006	0.282512	0.000011	0.282507	-9.2	-3.8	-3.4	0.4	1048	1518	-0.97
SK1A-04	258	0.031583	0.000283	0.001072	0.000006	0.282520	0.000018	0.282514	-8.9	-3.5	-2.8	0.6	1039	1501	-0.97
SK1A-05	243	0.032137	0.000444	0.001099	0.000013	0.282512	0.000013	0.282507	-9.2	-4.0	-3.6	0.5	1050	1526	-0.97
SK1A-06	258	0.038164	0.000081	0.001310	0.000003	0.282506	0.000013	0.282499	-9.4	-4.0	-3.5	0.5	1066	1535	-0.96
SK1A-07	255	0.025369	0.000089	0.000889	0.000005	0.282468	0.000014	0.282464	-10.7	-5.3	-4.8	0.5	1106	1616	-0.97
SK1A-08	257	0.031531	0.000110	0.001103	0.000005	0.282515	0.000013	0.282509	-9.1	-3.6	-3.2	0.5	1047	1512	-0.97
SK1A-09	257	0.023995	0.000233	0.000842	0.000007	0.282518	0.000013	0.282514	-9.0	-3.5	-3.0	0.4	1035	1502	-0.97
SK1A-10	255	0.039700	0.000043	0.001402	0.000004	0.282503	0.000013	0.282496	-9.5	-4.2	-3.7	0.5	1072	1543	-0.96
SK2A-01	256	0.045653	0.000464	0.001629	0.000018	0.282537	0.000014	0.282529	-8.3	-3.0	-2.5	0.5	1029	1468	-0.95
SK2A-02	233	0.061563	0.000585	0.002210	0.000021	0.282530	0.000019	0.282521	-8.5	-3.7	-3.1	0.6	1056	1502	-0.93
SK2A-03	245	0.046268	0.000667	0.001558	0.000025	0.282442	0.000015	0.282434	-11.7	-6.6	-6.0	0.5	1164	1688	-0.95
SK2A-04	260	0.034068	0.001092	0.001207	0.000036	0.282476	0.000019	0.282470	-10.5	-5.0	-4.3	0.7	1105	1599	-0.96
SK2A-05	245	0.077987	0.001253	0.002725	0.000044	0.282508	0.000017	0.282495	-9.3	-4.2	-3.8	0.5	1103	1550	-0.92
SK2A-06	262	0.048359	0.000520	0.001668	0.000012	0.282571	0.000017	0.282562	-7.1	-1.7	-1.1	0.6	983	1390	-0.95
SK2A-07	246	0.041070	0.000287	0.001468	0.000013	0.282526	0.000012	0.282519	-8.7	-3.6	-3.1	0.4	1041	1498	-0.96
SK2A-08	269	0.039191	0.000683	0.001352	0.000023	0.282484	0.000015	0.282477	-10.2	-4.5	-4.0	0.5	1098	1578	-0.96
SK2A-09	252	0.048659	0.000470	0.001641	0.000012	0.282535	0.000015	0.282527	-8.4	-3.1	-2.6	0.5	1034	1477	-0.95
SK2A-10	255	0.058865	0.000260	0.002054	0.000010	0.282518	0.000020	0.282508	-9.0	-3.7	-3.0	0.7	1069	1516	-0.94
SK12A-01	91	0.000273	0.000008	0.000008	0.000000	0.282426	0.000012	0.282426	-12.2	-10.4	-10.0	0.4	1138	1809	-1.00
SK12A-02	95	0.000397	0.000004	0.000012	0.000000	0.282482	0.000013	0.282482	-10.3	-8.2	-7.7	0.4	1062	1678	-1.00
SK12A-03	97	0.001037	0.000041	0.000032	0.000002	0.282550	0.000012	0.282550	-7.9	-5.7	-5.3	0.4	969	1523	-1.00
SK12A-04	93	0.000330	0.000006	0.000010	0.000000	0.282396	0.000015	0.282396	-13.3	-11.3	-10.7	0.5	1179	1871	-1.00
SK12A-05	94	0.000343	0.000009	0.000010	0.000000	0.282459	0.000013	0.282459	-11.1	-9.0	-8.6	0.5	1093	1730	-1.00
SK12A-06	92	0.000191	0.000010	0.000006	0.000000	0.282385	0.000015	0.282385	-13.7	-11.8	-11.3	0.5	1195	1900	-1.00
SK12A-07	97	0.000546	0.000037	0.000015	0.000001	0.282428	0.000013	0.282428	-12.2	-10.1	-9.6	0.5	1136	1798	-1.00
SK12A-08	95	0.000226	0.000005	0.000007	0.000000	0.282439	0.000012	0.282439	-11.8	-9.7	-9.3	0.4	1120	1774	-1.00

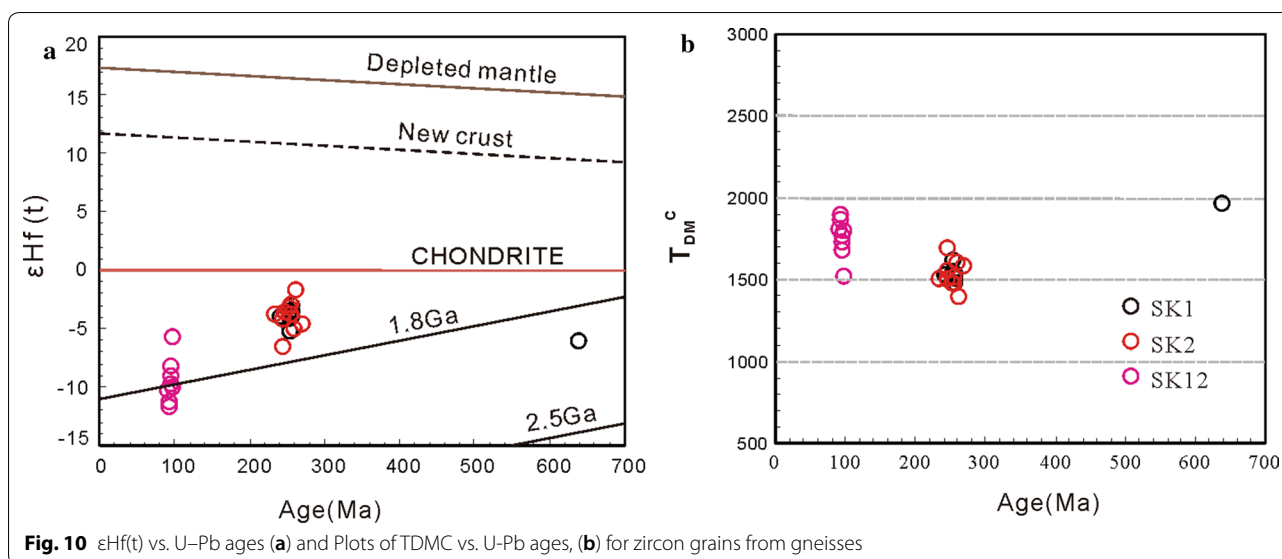


Fig. 10 $\epsilon\text{Hf}(t)$ vs. U–Pb ages (a) and Plots of T_{DM}^c vs. U–Pb ages, (b) for zircon grains from gneisses

earth elements (REE) for rock classification and petrogenetic interpretations (Winchester and Floyd 1977; Hastie et al. 2007).

The augengneiss samples (SK1 and SK2) have relatively high SiO_2 (66.0–76.3 wt%) and medium to high K_2O contents of 1.58–4.18 wt%. They are characterized by moderate contents of Al_2O_3 (14.4–16.1 wt%), $\text{Fe}_2\text{O}_3^{\text{T}}$ (1.58–4.18 wt%), and low TiO_2 (0.53–1.30 wt%), MnO (0.03–0.08 wt%), which are typical of metaluminous rocks according to the classification of Villaseca et al. (1998). All samples have $\text{Na}_2\text{O}/\text{K}_2\text{O}$ ratios less than 1 (0.58–0.70), and fall into the high-K calc-alkaline and calc-alkaline fields of the SiO_2 – K_2O diagram (Peccerillo and Taylor 1976) and the granodiorite field in the SiO_2 –($\text{Na}_2\text{O} + \text{K}_2\text{O}$) diagram (Middlemost 1994). According to the A–B classification after Debon and Le Fort (1983) the augengneisses are metaluminous. But as K, Na, and Ca, are mobile elements, migration of these elements may occur during metamorphism and thus affect the classification result, we also use the Th vs. Co diagram (Hastie et al. 2007) to classify the samples (Fig. 11), This diagram yields results that are consistent with major elements classification, suggesting no major alteration of whole-rock compositions.

In contrast, the leucogneiss samples SK12 and SK10 exhibit moderate Al_2O_3 (15.0–15.6 wt%) and low TiO_2 (0.07–0.11 wt%), MnO (0.05–0.10 wt%) and $\text{Fe}_2\text{O}_3^{\text{T}}$ (0.54–1.08 wt%) contents. All samples have a high $\text{Na}_2\text{O}/\text{K}_2\text{O}$ ratio, with sample SK10 of c. 1.9, sample SK12 of 1.2–0.85 with the former plotting in the calc-alkaline, the latter in the high-K calc-alkaline field of the SiO_2 – K_2O diagram (Peccerillo and Taylor 1976). The leucogneisses are peraluminous according to Villaseca et al. (1998) and

the A–B classification of Debon and Le Fort (1983), and plot into the granite field in the SiO_2 –($\text{Na}_2\text{O} + \text{K}_2\text{O}$) diagram (Middlemost et al. 1994). Also, according to the Co–Th diagram (Hastie et al. 2007) the leucogneisses are high-K calc-alkaline rocks.

The trace element contents of the two groups show quite different patterns with the augengneisses in general more enriched than the leucogneisses. In primitive-mantle-normalized multi-element diagrams (McDonough and Sun 1995), both groups of gneisses show enrichment in large-ion lithophile elements (LILEs; e.g., Cs, Rb, and K) with pronounced negative anomalies of Nb and P, (Fig. 12a). The augengneisses display also relative negative anomalies for Ba, Sr and Eu. Compared with augengneiss samples with positive anomalies for Ti and high $\text{La}_\text{N}/\text{Yb}_\text{N}$ ratios (15.4–33.6), the leucogneiss samples display lower normalized light REE abundances and pronounced negative anomalies for Ti as well as lower $\text{La}_\text{N}/\text{Yb}_\text{N}$ ratios (0.42–8.27). In addition, they display positive anomalies for U, K, and Sr. Positive and negative Ti anomalies in analyzed augengneisses and leucogneisses, respectively, are interpreted to be due to the extraction of Ti in biotite crystallizing in augengneiss during the melt evolution.

Chondrite-normalized REE patterns are plotted in Fig. 11b, and display for all augengneiss samples high total contents (182.7–275.5 ppm; Table 3), whereas leucogneisses have much lower REE contents (18.0–57.9 ppm; Table 3). Augengneisses have especially much more enriched LREE contents than leucogneisses and show a strong decrease in enrichments from light to heavy REEs. Leucogneisses show also a decrease of enrichments of LREE and almost flat HREE patterns. These patterns are

Table 3 Whole-rock major and trace element data of the Pohorje samples

	SK1A	SK1B	SK1C	SK1D	SK1E	SK1F	SK2A	SK10A-1	SK12A	SK12B	SK12C	SK12D	SK12E
	Augen-orthogneisses (SK1, SK2)						Biotite-gneisses (SK12)						
SiO ₂	67.85	65.99	67.96	68.38	66.24	67.93	71.41	76.00	74.73	73.23	73.06	73.27	73.26
TiO ₂	0.59	0.55	0.55	0.56	0.65	0.60	0.32	0.07	0.07	0.10	0.10	0.11	0.10
Al ₂ O ₃	14.98	16.05	14.99	14.78	15.58	14.54	14.41	15.60	14.99	15.45	15.38	15.28	15.36
Fe ₂ O ₃ T	3.64	3.38	3.39	3.51	4.18	3.73	1.58	0.54	0.54	1.01	1.03	1.08	0.99
MnO	0.07	0.07	0.07	0.07	0.08	0.08	0.03	0.10	0.06	0.06	0.06	0.05	0.06
MgO	1.18	1.13	1.13	1.12	1.30	1.23	0.53	0.13	0.13	0.24	0.25	0.27	0.25
CaO	2.42	2.17	1.96	2.34	2.57	2.18	1.11	1.47	1.65	2.25	2.24	2.32	2.26
Na ₂ O	2.92	2.75	2.52	2.87	2.98	2.62	2.33	3.72	3.69	4.13	4.07	4.14	4.13
K ₂ O	4.60	6.14	5.66	4.66	4.67	4.97	7.27	2.06	4.36	3.91	3.86	3.54	3.75
P ₂ O ₅	0.21	0.22	0.20	0.20	0.26	0.22	0.12	0.01	0.02	0.03	0.03	0.04	0.03
LOI	0.85	1.05	1.07	0.88	0.83	0.97	0.74	1.20	0.57	0.39	0.34	0.43	0.43
Total	99.30	99.50	99.50	99.38	99.34	99.07	99.86	100.91	100.81	100.80	100.43	100.53	100.62
K ₂ O/Na ₂ O	1.58	2.23	2.25	1.62	1.57	1.90	3.12	0.55	1.18	0.95	0.95	0.85	0.91
Li	23.76	20.38	20.46	25.46	20.98	21.28	11.40	3.25	5.98	24.36	24.21	29.92	18.76
Be	2.37	2.27	2.17	2.45	2.26	2.15	1.02	5.07	5.26	3.05	3.14	3.37	3.41
Sc	7.07	7.08	7.93	9.52	6.81	7.34	3.39	2.86	1.65	2.12	2.27	2.42	2.07
Ti	91229	97721	91281	89937	94788	88853	87178	401	429	569	591.19	661.15	592.93
V	58.44	58.05	39.54	43.63	47.09	50.65	43.81	6.51	1.54	5.78	5.06	8.39	5.77
Mn	523.46	534.80	557.17	632.84	530.62	593.67	255.63	702.46	368.05	417.96	494.42	330.69	472.55
Co	6.31	7.61	6.42	7.22	5.69	6.39	3.17	0.59	0.41	0.69	0.70	0.75	0.76
Ni	16.77	73.69	28.66	20.99	13.86	15.91	21.62	3.99	4.96	3.47	4.13	2.79	1.08
Cu	4.37	17.60	9.78	7.77	5.30	10.74	2.17	2.92	3.03	3.95	4.17	4.15	7.42
Zn	70.02	54.75	54.27	123.83	65.09	58.47	25.61	7.52	16.56	65.06	33.17	32.75	28.57
Ga	20.77	20.72	20.48	22.17	20.02	20.14	15.80	14.50	11.80	14.38	14.74	15.40	13.80
Rb	210.21	232.10	222.45	212.91	207.89	206.95	232.04	57.53	125.65	115.89	115.52	113.77	111.61
Sr	205.26	275.96	249.31	248.73	205.28	234.05	244.98	115.13	200.53	529.51	522.59	541.03	510.50
Y	29.34	23.83	26.45	27.27	27.74	26.18	9.92	26.12	12.54	14.70	17.48	10.99	15.74
Zr	276.48	260.36	296.08	296.10	257.56	274.09	152.35	28.08	35.60	67.45	69.95	76.78	63.89
Nb	20.35	19.14	20.07	22.58	19.37	21.60	13.15	9.30	8.88	12.95	12.58	14.22	12.68
Mo	0.94	1.31	0.77	0.59	1.00	0.48	0.35	1.48	0.19	0.48	0.15	0.16	0.15
Sn	3.22	2.80	2.84	3.13	3.15	2.94	1.19	1.20	1.15	0.93	0.93	0.95	0.72
Cs	7.57	6.97	6.74	8.67	7.05	7.26	3.21						
Ba	656.08	1028.2	996.92	695.74	655.85	890.54	1057.5						
La	61.07	45.81	60.74	51.36	57.26	59.65	41.17	7.66	5.86	9.60	10.99	12.32	9.10
Ce	121.55	92.08	121.61	105.56	113.93	119.80	83.49	17.19	11.04	17.36	20.44	23.19	16.55
Pr	13.49	10.39	13.61	11.84	12.73	13.42	8.97	2.29	1.26	1.97	2.26	2.62	1.82
Nd	49.65	38.83	49.70	44.11	47.25	49.44	32.65	10.31	5.00	7.54	8.63	10.01	7.02
Sm	9.01	7.40	8.95	8.27	8.57	8.84	6.15	3.23	1.39	1.68	1.93	2.19	1.54
Eu	1.21	1.11	1.23	1.07	1.20	1.16	1.17	0.24	0.31	0.50	0.52	0.50	0.49
Gd	7.06	5.84	6.74	6.57	6.72	6.67	4.30	3.00	1.61	1.80	2.04	2.07	1.65
Tb	0.95	0.79	0.89	0.90	0.91	0.91	0.48	0.61	0.33	0.36	0.40	0.35	0.32
Dy	5.16	4.34	4.84	4.94	4.89	4.91	2.05	4.23	2.18	2.33	2.74	1.98	1.92
Ho	0.94	0.79	0.87	0.91	0.90	0.88	0.32	0.85	0.42	0.49	0.58	0.36	0.44
Er	2.58	2.22	2.42	2.55	2.49	2.46	0.88	2.46	1.15	1.38	1.71	0.97	1.25
Tm	0.34	0.30	0.32	0.35	0.34	0.35	0.12	0.39	0.17	0.21	0.26	0.14	0.20
Yb	2.15	1.96	2.09	2.30	2.05	2.23	0.82	2.89	1.16	1.47	1.81	1.00	1.31
Lu	0.32	0.29	0.30	0.34	0.31	0.33	0.13	0.42	0.17	0.21	0.26	0.15	0.20
Hf	6.82	6.50	7.35	7.44	6.48	6.89	3.47	1.54	1.38	2.34	2.45	2.73	2.21

Table 3 (continued)

	SK1A	SK1B	SK1C	SK1D	SK1E	SK1F	SK2A	SK10A-1	SK12A	SK12B	SK12C	SK12D	SK12E
Ta	1.44	1.47	1.62	1.73	1.50	1.80	0.70	0.64	1.01	0.66	0.63	0.72	0.70
W	0.47	0.55	0.53	0.42	0.51	0.74	0.39	0.25	0.25	0.38	0.13	0.79	0.07
Pb	39.09	45.00	38.56	35.99	38.67	35.62	67.04	34.95	57.29	63.09	63.07	61.36	62.99
Bi	0.43	0.27	0.29	0.27	0.41	0.35	0.14						
Th	25.73	17.48	23.98	22.37	25.47	22.92	20.22	5.18	3.95	4.99	6.21	6.67	4.74
U	5.11	3.83	4.56	4.36	5.01	4.24	2.13	9.25	3.17	7.42	9.09	6.20	6.18
ΣREE	275.47	212.13	274.31	241.07	259.56	271.03	182.71	55.77	32.06	46.9	54.58	57.85	43.81
(La/Yb) _N	19.14	15.77	19.59	15.04	18.8	18.06	33.69	1.79	3.4	4.41	4.09	8.27	4.67
La/Lu	191.07	160.34	199.70	152.04	184.01	183.37	307.35	18.25	35.26	45.33	42.63	79.73	46.24
Sr/Y	7.00	11.58	9.43	9.12	7.40	8.94	24.69	4.41	15.99	36.02	29.89	49.21	32.42
Eu/Eu*	0.47	0.51	0.49	0.44	0.48	0.46	0.69	0.23	0.63	0.88	0.8	0.72	0.95

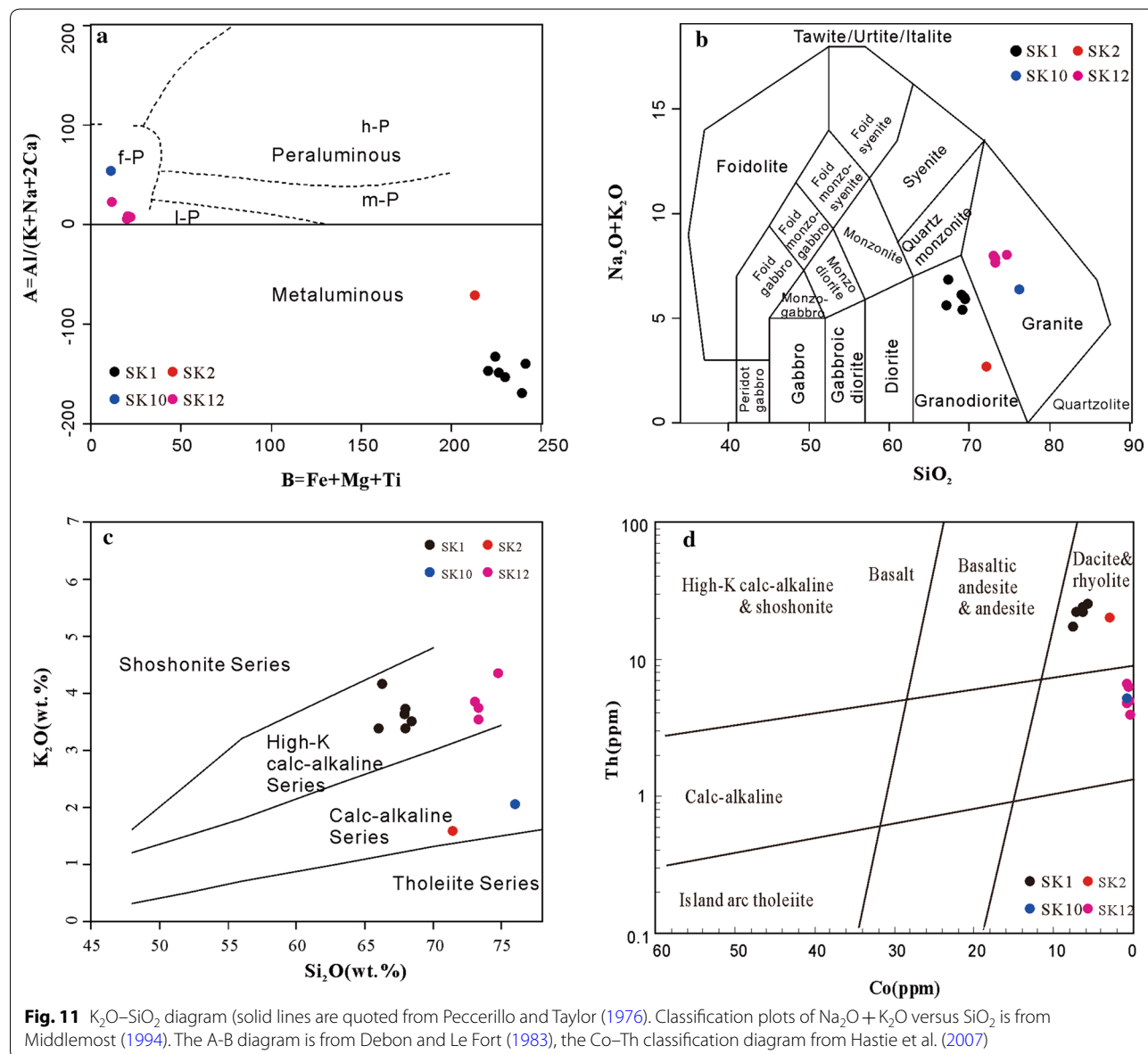
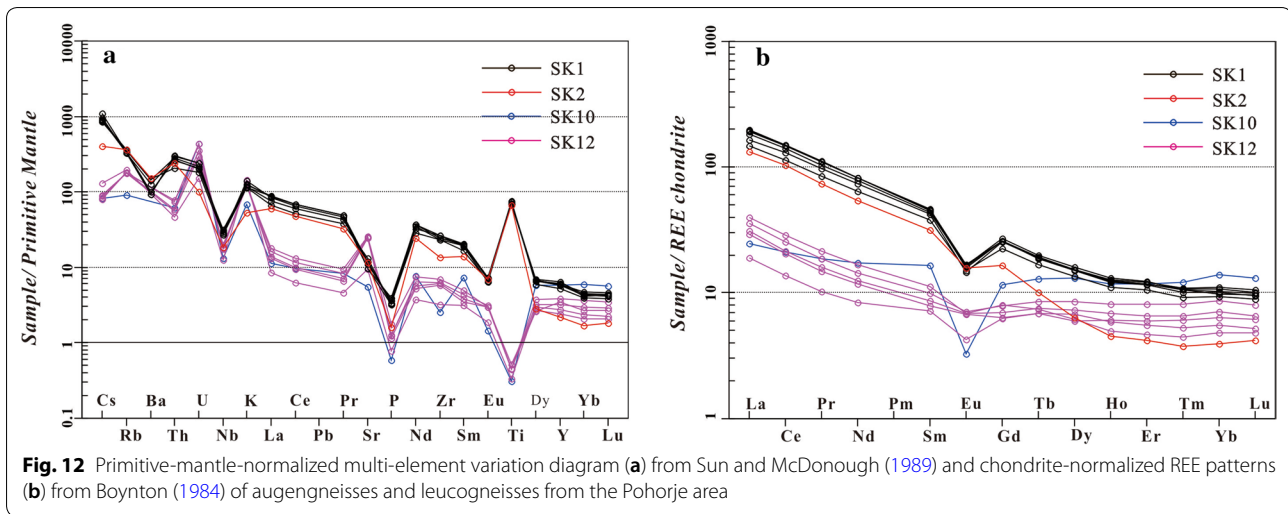


Fig. 11 K_2O-SiO_2 diagram (solid lines are quoted from Peccerillo and Taylor (1976). Classification plots of $Na_2O + K_2O$ versus SiO_2 is from Middlemost (1994). The A-B diagram is from Debon and Le Fort (1983), the Co-Th classification diagram from Hastie et al. (2007)



also expressed in the $(\text{La}/\text{Yb})_N$ ratios (Table 3) with about 15–20 for the augengneisses (one sample 34) and about 2–8 for the leucogneisses (one sample 0.4). Sr/Y ratios show also large differences between the two groups with 7–12 (one sample 25) for augengneisses and 16–49 (one sample 5) for the leucogneisses. The augengneisses have strong negative Eu anomalies with a narrow range of Eu/Eu^* ratios of 0.44–0.51 with the exception of one sample with 0.69 (Table 3). Leucogneisses have smaller negative Eu anomalies with Eu/Eu^* ratios of 0.63–0.95. However, one analysis of the leucogneiss sample SK10 displays a very flat REE pattern and the most pronounced negative Eu anomaly with a Eu/Eu^* of 0.23.

Specifically, the augengneisses plot mostly in the field of A-type granite in the $\text{Zr} + \text{Nb} + \text{Ce} + \text{Y}$ vs. FeOt/MgO and $(\text{Na}_2\text{O} + \text{K}_2\text{O})/\text{CaO}$ diagrams of Whalen et al. (1987) (Fig. 13). In the $\text{Nb}-\text{Y}-3$ Ga diagram of Eby (1992), which allows a further division of A-type granites, four samples of augengneiss plot in the A1 field, another sample in the A2 field. Samples SK1 plot only just in the field A2, the field of post-collisional to post-orogenic setting, sample SK2 in the field A1, the field for rift- to plume-related granites (Eby 1992).

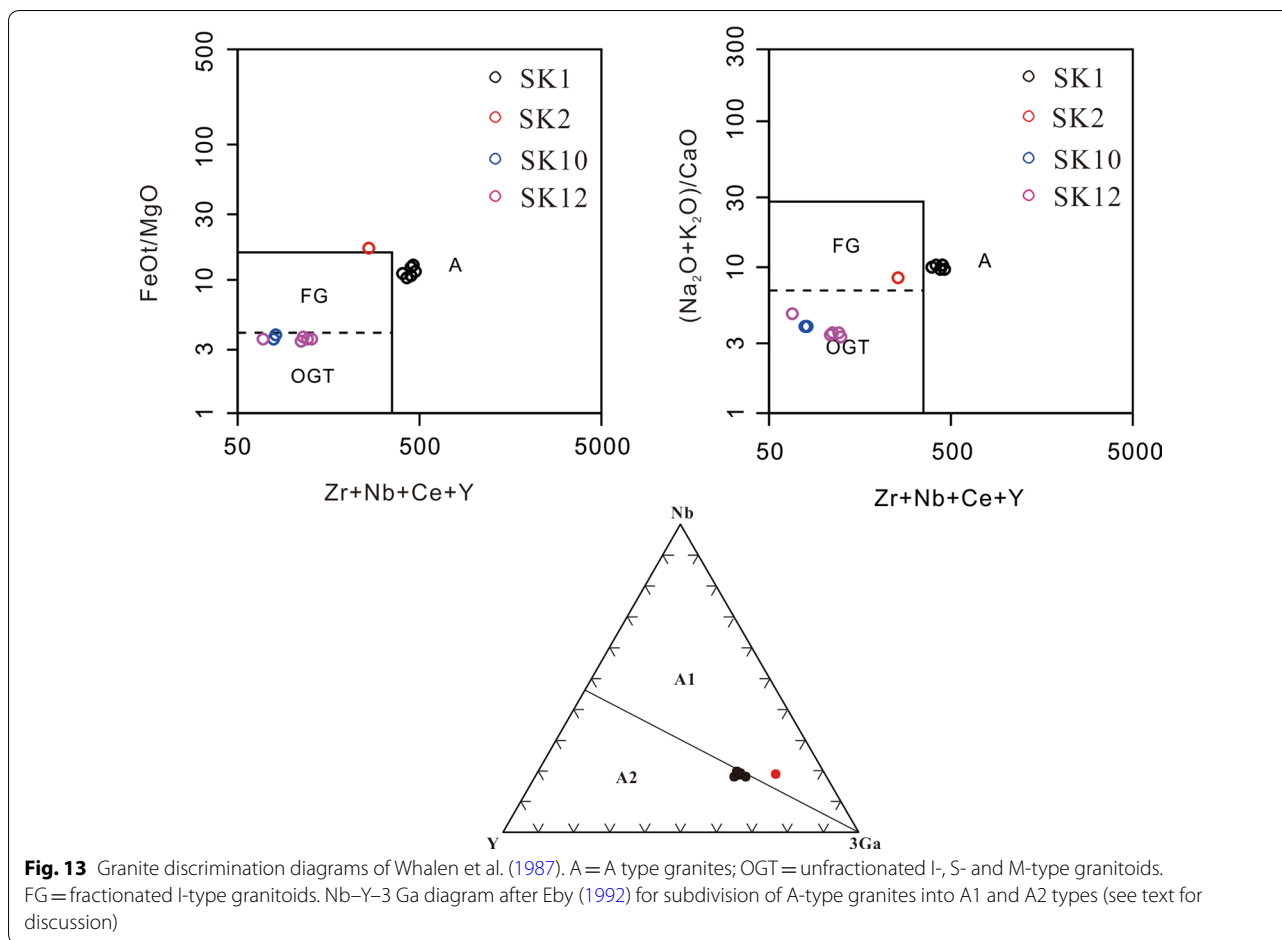
6 Discussion

The study demonstrates that the two orthogneiss groups show very different characteristics in geochemistry, properties of zircons and their U–Pb ages and also in the type and metamorphism of their country rocks. We will therefore discuss first the differences of the two groups, then the significance of the zircon ages and the petrogenesis of the two groups separately and then their relationship and the consequence for the geodynamics interpretation of the Austroalpine unit and the Pohorje area in particular. There are strong indications that the two orthogneiss

groups belong to two different Alpine tectonic units, not to a coherent unit as assumed by most previous researchers (e.g. Kirst et al. 2010, Janák et al. 2015), which would of course have implications for the interpretation of the genesis and setting of the two plutonic suites, the main topic of this paper. A detailed mapping and the discussion of the Alpine tectonic evolution of the two supposed units is subject of further investigations.

6.1 Differences between augengneiss and leucogneiss

The augengneisses and leucogneisses were overprinted during the Alpine metamorphism with variable intensity leading to various structural and chemical changes to the magmatic features. The microfabrics of augengneisses with recrystallization of feldspars indicate deformation at at least upper greenschist facies conditions, but do not allow tight constraints on deformation temperatures. But the stability and recrystallization of biotite and plagioclase, and the absence of HP to UHP minerals in augengneisses, as white mica, garnet or rutile, indicate medium-pressure conditions during the Alpine metamorphism. This metamorphic facies is also indicated by the assemblage Pl-Hbl in amphibolites and especially the paragenesis of St-Grt-Ms-Pl-Ky-Sil-Bt in micaschists (own observations). The well preserved magmatic zircons of the augengneiss, in contrast to the metamorphic (re)crystallized zircons in the investigated leucogneiss samples is a further strong hint that the two orthogneiss groups experienced quite different PT conditions during the Cretaceous metamorphic overprint. We consider, therefore, that two tectonic units are exposed in the southernmost Pohorje: (1) EGU with UHP/HP metamorphism hosting the leucogneisses and (2) the augengneiss-bearing unit, which is associated with micaschists, with amphibolite facies-grade metamorphism.



6.2 Age and petrogenesis of augengneiss

The augengneiss body is dated at approximately 255–260 Ma on zircon by U–Pb LA-ICP-MS (Fig. 7; Additional file 1: Table S1), which is Late Permian according to the International Chronostratigraphic Chart v2020/01 of the ICS (Cohen et al. 2013). The mostly porphyric granodiorites intruded into a sequence of gneisses, micaschists, marbles and amphibolites.

The magmatic protolith of the augengneisses is a metaluminous granodiorite, which shows several characteristics of A-type granites as a strong enrichment in incompatible trace elements, including LILE and HFSE, but a relative depletion of Ba, Sr, and Eu that are compatible with fractionation of feldspars, as well as a strong depletion of P by fractionation of apatite (Eby 1990; Bonin 2007). Due to the high contents of the HFSE $Zr + Nb + Ce + Y$ this orthogneiss plots in the field of A-type granites in the classification of Whalen et al. (1987) and belongs to the ferroan A-type group according to Frost et al. (2001). In the subdivision of A-type granites based on Y/Nb ratios by Eby (1992) the augengneisses straddle the field boundary between

type A2 and A1 or plot into field A1. Most petrogenetic models for A-type granites postulate either a postcollisional setting with melting of continental crust that has experienced a preceding episode of melt extraction during continent–continent collision or the differentiation of oceanic-island like mantle melts in a rift setting (Whalen et al. 1987; Eby 1990, 1992; Bonin 2007). The former should give rise to A2-type, the latter to A1-type granites (Eby 1992). The Y/Nb ratios of the augengneisses on the boundary of A1 and A2 fields fits very well a model with melting of a continental crust, which has undergone a cycle of continent–continent collision during the Variscan orogeny about 60 Ma earlier. The initiation of rifting and the probable involvement of mantle melts should shift the granitoids from the field A2 towards the field A1.

Hf isotopic data show $\epsilon Hf(t)$ values of -13.7 to -7.9 , and Hf crustal model ages (T_{DM}^C) of 969–1195 Ma suggesting the derivation of melts from Proterozoic continental crustal source. The continental source is also demonstrated by inherited Proterozoic cores of magmatic zircons.

The Permian intrusion age of augengneiss is related to Permian continental extension, which follows the Variscan orogeny within a few tens of million years (Kozur 1991; Neubauer et al. 2000; Putiš et al. 2018) (Fig. 14).

At present, it is unknown whether the host rocks of augengneisses also experienced the Permian–Triassic low-P/high-T metamorphism as known from the EGU (Habler and Thöni 1998; Thöni and Miller 2000) (Table 3). As already discussed above, the excellent preservation of Permian zircon ages within an amphibolite-facies grade area indicates that the augengneiss body escaped high temperatures of 800–850 °C typical for the UHP/HP metamorphic conditions in the south-west (Janák et al. 2015; Table 4).

6.3 Age and metamorphism of leucogneiss

The leucogneisses are heterogeneously composed and, as part of the EGU, are associated with eclogites, paragneisses, micaschists and ultramafic cumulates of oceanic affinity (SBUC). Previous studies indicate Cretaceous eclogite facies metamorphic overprint for the EGU in the south-eastern Pohorje Mountains, with P–T conditions in the range of 3.0–3.7 GPa and 700–940 °C (Janák et al. 2004, 2009, 2015; Vrabec et al. 2012; Table 4 for further data). These conditions are also substantiated by findings of microdiamonds in metasedimentary rocks, which give UHP P–T conditions of ≥ 3.5 GPa and 800–850 °C (Janák et al. 2015). These P–T conditions make it essential to consider this young metamorphic event when interpreting isotopic data from the “pre-Alpine basement”.

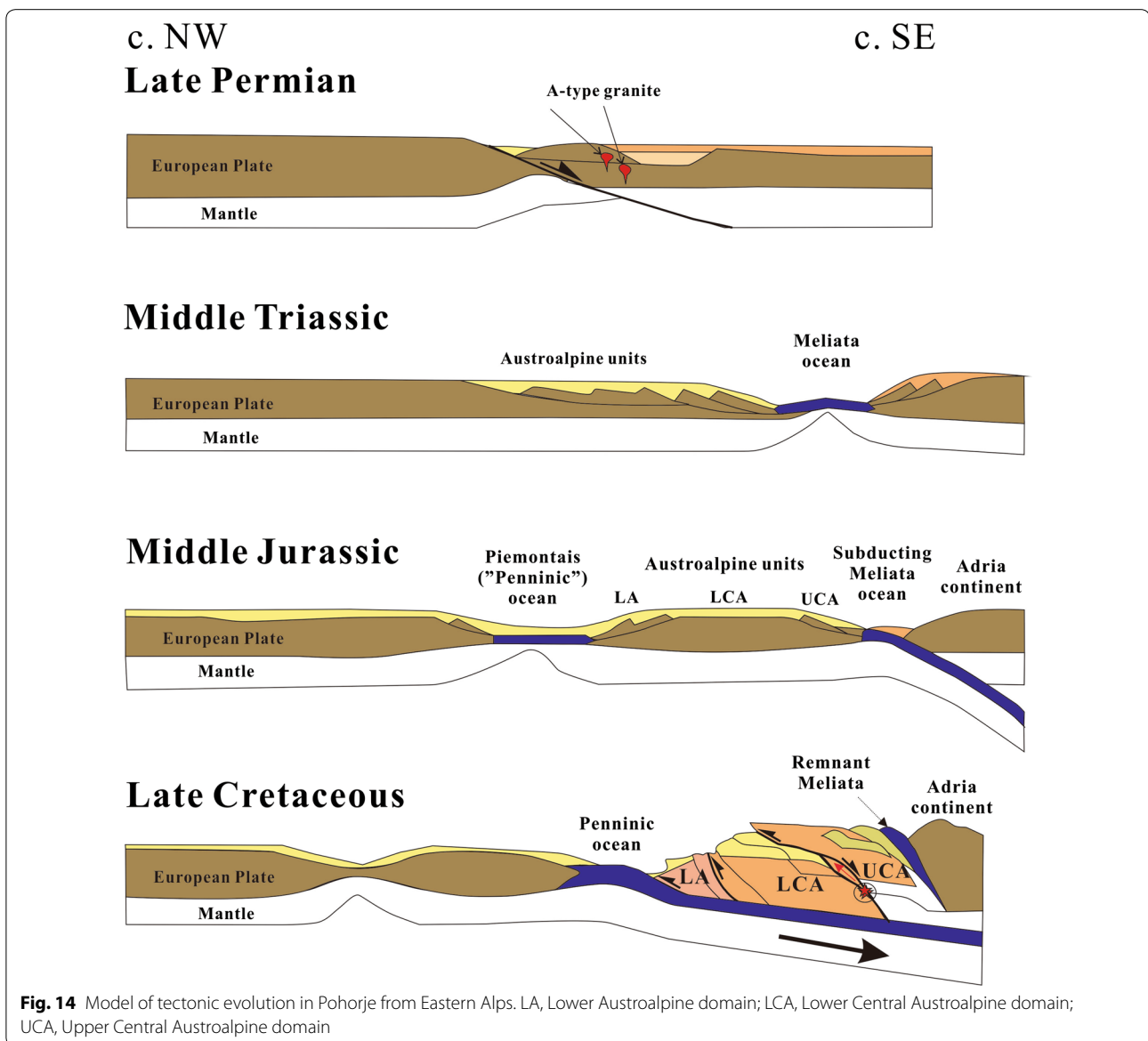


Table 4 P-T conditions of EGU from previous research

Igneous Rocks	Age	P (GPa)	T (°C)	References
Mica schists	320–280	0.6–0.8	650	Schulz 2017
Mica schists	275 ± 25	0.24–0.42	530	Schuster 2015
Garnet mica schists	269.2 ± 6.2	0.46	540	Thöni and Miller 2009
Mica gneiss	250–270	0.38–0.4	590–600	Habler and Thöni 2001
Mica gneiss	249 ± 3	0.38–0.65	600–650	Schorn 2018
Eclogites	90	2.4	700–730	Miller et al. 2007
Garnet lherzolite	87–93	4	900	De Hoog et al. 2009
Eclogites	87–95	2.4–2.5	640–740	Thöni et al. 2008a, Table 1
Eclogites	90	2.4	630–650	Miller et al. 2007
Eclogites	90.7 ± 1	2.1	750	Miller et al. 2005a
Eclogite facies		2.4	650–730	Miller 1990
Gneiss	92.5	2.2–2.7	700–800	Janák et al. 2009
Gneiss	92–95	3.5	800–850	Janák et al. 2015
Kyanite-eclogite	92	3.0–3.7	710–940	Vrabec et al. 2012
Eclogite	94–95	2.2	630–740	Thöni et al. 2008b
Eclogites	Cretaceous	1.8–2.5	630–700	Sassi et al. 2004
Garnet peridotites	Cretaceous	3.4–4	890–960	Janák et al. 2006
Kyanite eclogites	Cretaceous	3.0–3.1	760–825	Janák et al. 2004
Eclogites	–	2.5	750–800	Hauzenberger et al. 2016
Garnet lherzolite	91.6 ± 4.1	4	900	Sandmann et al. 2016

The dated leucogneiss samples were collected nearby to localities where diamond was found by Janák et al. (2015). Consequently, we argue that these high temperatures of 800–850 °C were responsible for new crystallization of broad zircon rims obliterating the older record of magmatic and inherited ages in most zircon grains. Zircons from the leucogneisses have also similar features such as rounded shapes and a faint internal zonation with some preserved cores as zircons from eclogites (Miller et al. 2005b) and metapelites (Janák et al. 2009). The Cretaceous ages of the zircons are also consistent with ages for the UHP metamorphism obtained with Sm–Nd (Miller et al. 2005b) and Lu–Hf (Thöni et al. 2008; Sandmann et al. 2016) dating.

The fabric of leucogneisses shows dynamic recrystallization of quartz and plagioclase. Two types of recrystallization mechanisms can be inferred from the microstructures of quartz (Passchier and Trouw 2005). Highly irregular grain boundaries, pinning structures, and leftover grains in quartz indicate grain boundary migration (Fig. 3). Additionally, small, uniform sized, slightly elongated quartz and feldspar grains argue for subgrain rotation. These observations are consistent with deformation during retrogression within amphibolite and greenschist conditions during retrogression subsequent to Cretaceous eclogite facies metamorphism, and nearly no record of UHP/HP metamorphic fabrics can be observed within the studied leucogneisses. Similar

retrogressive fabrics overprinting eclogite-facies fabrics were also observed in more northern areas of EGU (Thöni and Miller 2000; Habler et al. 2007; Thöni and Miller 2010).

The dated leucogneisses give metamorphic ages of 89–90 Ma by zircon U–Pb LA-ICP-MS dating (Fig. 8; Additional file 1: Table S1), the same age as all eclogites in the EGU. The ages of inherited zircon grains range between 260 ± 3.3 Ma and 1489 ± 31.9 Ma, the minimum inherited ages are similar as those of augengneiss samples. The mode of ages for core analyses of ca. 265 Ma of sample SK10 and the single youngest core age of 260 Ma of sample SK12 are a tentative formation age of these meta-granites. A more definite age would require analysis of more cores and probably samples, which zircons are less overprinted by the Alpine UHP conditions. However, a Permian age for the leucogranites is quite reasonable based on the Permian low pressure, high temperature metamorphism within EGU (Habler and Thöni 2001; Thöni and Miller 2009; Schuster et al. 2015; Schulz 2017; Schorn 2018), magmatic activity as gabbro intrusions of proven Permian age (Thöni and Jagoutz, 1992) and pegmatites (Knoll et al. 2018 and references therein) in the EGU.

Geochemically, the leucogneisses are very different from the augengneisses. Based on major element compositions, they are peraluminous, high-K calc-alkaline granites, supported also by more robust Co-Th contents.

Trace element patterns show much lower enrichments than the augengneisses, with the exception of U, K and Sr and also negative anomalies of Nb and P. Ti is strongly depleted in the leucogneisses, in contrast to the augengneisses which are strongly enriched in Ti. REEs show much less enrichment in LREE and almost flat HREE patterns and also only weak negative Eu anomalies (with the exception of one analysis).

We consider that this segment of the EGU is part of the distal Late Permian rift zone (Fig. 14). The zircon ages indicate that the UHP/HP metamorphism event occurred in the early Late Cretaceous (ca. 90 Ma).

6.4 Relationship of augengneisses and leucogneisses

As discussed before, the two orthogneiss groups display major differences in their petrology and geochemistry, their metamorphic overprint and also their country rocks. However, all previous investigators consider the south-eastern part of the Pohorje area as a coherent tectonic unit that underwent Alpine UHP metamorphism. We argue for the presence of two nappe units that experienced quite different Alpine metamorphic conditions but also show differences in their internal composition. The main difference is the UHP conditions with very high temperatures of the EGU and amphibolite conditions with no hints for high or even ultrahigh pressure conditions of the unit containing the augengneisses. These differences are also expressed in the orthogneisses themselves, with the paragenesis Bt + Plag in the augengneiss vs. Ms + Grt in the leucogneiss and also the very different appearance of zircon with well-preserved magmatic zircons in augengneiss and strongly overprinted/regrown zircon in the leucogneiss. The country rocks of the two gneiss groups show the same differences in metamorphic conditions. Rocks of the EGU show parageneses, which give UHP conditions as described by numerous investigators before, the country rocks of the augengneisses show paragenesis of amphibolite conditions without hints for HP conditions.

The boundary between the two tectonic units should roughly coincide with the tail of the Miocene granodiorite intrusion (Fig. 3). All described samples which gave UHP conditions are from the area south-west of the Miocene intrusion (Radkovec–Visole) with the exception of some eclogites south of Sp. Prebukovie, related with the ultramafic body and the eclogites and their retrogressed amphibolites. The augengneisses east of the Miocene granite are associated with paragneisses, micaschists, amphibolites and marbles, which show amphibolite metamorphic conditions. Amphibolites there show no relics of eclogite conditions but well-equilibrated equigranular microstructures, whereas amphibolites retrogressed from eclogite display symplectitic microstructures with

a wide range of amphibole grain sizes on the cm-scale. Marbles seem to be typical for the amphibolite facies unit (Vrabec et al. 2018 and geological maps of Mioč and Žnidarčič 1977; and Žnidarčič and Mioč 1989) and are not described from the unequivocal UHP unit. For a definite delineation of the boundary and the characterization of its nature clearly more field work is required. If the interpretation of the different metamorphic evolution holds, it must be a tectonic boundary, either a thrust or detachment fault, that brought two tectonic units with very different Alpine pressure conditions together, thus different subductions depths, in contact at probably amphibolite facies conditions.

According to the mapping and structural analysis by Kirst et al. (2010) two tectonic relations are possible. They mapped two antiforms, the overturned to recumbent Slovenska Bistrica Antiform with the SBUC as its core and the upright Pohorje Antiform to the east (see Fig. 2). The investigated area is on the western limb of the young Pohorje Antiform, with a general dip of foliations to the south (see Figs. 3 and 8 in Kirst et al. 2010). Therefore, the augengneiss unit is now in the footwall of the UHP-unit. This could be the primary relationship, with the UHP unit thrust onto the augengneiss unit. The second possibility is that the augengneiss unit is entangled in the Slovenska Bistrica Antiform and is part of the overturned limb. It would thus be in a hangingwall position before the recumbent folding. These alternatives have of course implications for the parallelization with other Austroalpine units further north. In the area of the Kor- and Saualpe there are marble-bearing amphibolite facies units without HP conditions both over- and underlying the EGU (Kurz et al. 2002; Thöni 2006; Wiesinger et al. 2006; Schorn and Stüwe 2016).

6.5 Tectonic setting of Permian rift-related magmatic rocks

We consider the Pohorje segment of the EGU and of the augengneiss unit are part of the Permian rift zone.

The Eastern Alps and their extension in south-eastern and eastern Europe comprise the Austroalpine domain of continental affinity, which is characterized by a Middle Triassic passive continental margin succession, which opened towards the Meliata Ocean (Channell and Kozur 1997; Lein 1987; Neubauer et al. 2000; Schmid et al. 2004; Kirst et al. 2010; Plašienka 2018). However, there is not much data on the Early Permian to Early Triassic rift development, which finally formed the Meliata Ocean. Many researchers proposed that Alpine tectonic evolution started with onset of Early Permian rifting immediately followed by carbonate platform in the Southalpine unit (Schaffhauser et al. 2015) formed after deposition of the post-Variscan, Upper Carboniferous (Pennsylvanian) molasse. Much evidence for Permian rift magmatism

and high-temperature metamorphism is also found in Western and Southern Alps (Schaltegger and Brack 2007; Kunz et al. 2018; Manzotti et al. 2018). For EGU, further evidence of divergence and extension of the lithosphere was the emplacement of tholeiitic gabbros (Thöni and Jagoutz 1992; Schuster and Stüwe 2008; Kirst et al. 2010; Herg and Stüwe 2018), a few leucogranites (Morauf 1980; Tropper et al. 2007; Knoll et al. 2018) and low-pressure, high-temperature metamorphism within EGU (Table 4 for references). Knoll et al. (2018) argue for a derivation of widespread, often Lithium bearing pegmatites from small leucogneiss bodies within and in the footwall of EGU. In this study, we found evidence of A-type granite formation from our augengneiss samples, which could be also the source of pegmatites. The $\epsilon_{\text{Hf}}(t)$ values of zircons are negative (-6.4 to -1.7) suggesting that our samples formed by partial melting of old continental crust. So, we suggest that the rifting and lithospheric thinning in the Permian occurred by north–south extension (in present-day coordinates) in response to westward propagation of the Neotethys ocean. Crustal melting caused granite and pegmatite intrusions at mid-crustal levels within the future EGU. Our orthogneisses could be considered as the source magma of seemingly rootless Late Permian (to Triassic) pegmatites widespread within the EGU in the surroundings of the study area (Kirst et al. 2010) and further to the north. We argue that EGU (and underlying and overlying units) represent middle-lower parts of a boudin-like stretched continental crust, within which older fabrics are partly well preserved similar as observed in recent passive margins (Clerc et al. 2015). In that case, our data imply that the stretched continental crust of EGU as part of the Permian rift with magmatic rocks (and the subsequent) Triassic passive margin was potentially not much wider than ca. 100 km, was then subducted and subsequently rapidly exhumed during early Late Cretaceous times.

6.6 Continental subduction

The age data summarized in Table 4 and the ages of the leucogneiss samples suggest that the UHP/HP metamorphism event occurred in 89.34 ± 0.69 Ma and 90.8 ± 1.2 Ma, as has been widely reported (Miller et al. 2005b; De Hoog et al. 2011; Knoll et al. 2018). Janák et al. (2015) considered that the Pohorje nappe reached maximum depth at c. 95–92 Ma. The subduction zone formed during Early Cretaceous in the northwestern foreland of the Meliata suture after Late Jurassic closure of the Meliata Ocean and the resulting collision, by progressive subduction of the Triassic passive margin with the associated Permian rift lithologies, when southeastward, intra-oceanic subduction of the Meliata Ocean terminated in collision of the Austroalpine continental margin with the

accretionary prism associated with this subduction. During the Early Cretaceous, intracontinental subduction zone continued within the Austroalpine continental crust at the site of a Permian-aged rift (Janák et al. 2004, 2015; Stüwe and Schuster 2010).

Previous research also demonstrates that the Lower Central Austroalpine Units were subducted in an intracontinental subduction zone after complete subduction of the Meliata Ocean and the following continent collision, increasing towards SE (in present-day coordinates) and reaching more than 100 km depth in the Pohorje Mts., and exhumation of the Pohorje nappe at ca. 90 Ma (Froitzheim et al. 2008). For the geodynamics of exhumation, several models were proposed: (1) slab break-off (Neubauer et al. 2000), and (2) downward extraction of the Meliata oceanic slab (Froitzheim et al. 2008), which carried the Upper Central Austroalpine continental units in its northwestern part (Froitzheim et al. 2008). In this model, the latter units breakoff caused a reduction in horizontal stress along its trailing edge and thereby promoted exhumation of deeply subducted and directly emplaced on the UHP rocks, the SBUC was part of the down-going plate from the beginning (Kirst et al. 2010). On the other hand, footwall accretion of Austroalpine nappes during Cretaceous (between ca. 120 and 75 Ma) was already proposed by Dallmeyer et al. (1998). E.g., the Lower Austroalpine nappes were incorporated into the thrust belt during late Cretaceous (Neubauer 1994) and units from the Penninic ocean during Eocene (Liu et al. 2001). Consequently, a continuous slab could have caused subduction and the Austroalpine passive margin is entirely consumed, and no slab-break-off is needed to explain the Austroalpine nappe structure. This model is shown in Fig. 14 for the Late Cretaceous. There is a significant difference to previous models of, e.g., Froitzheim et al. (2003) and Janák et al. (2009), which assumes several distinct slabs and slab extraction during Late Cretaceous. As Dallmeyer et al. (1998) have shown, the Austroalpine nappe complex accreted by footwall propagation of thrusting continuously between ca. 110 Ma and 78 Ma. This observation implies that always the same heavy mantle slab is the driving force for thrusting and frontal nappe accretion and no interruption by slab extraction is needed to explain accretation of Meliata remnants and Austroalpine continental units.

7 Conclusions

- (1) The Pohorje area contains two groups of distinct orthogneisses which represent part of Permian granitic to granodioritic bodies which are dated at 255–260 Ma and are derived from partial melting of lower continental crust in a rift zone.

- (2) An intracontinental subduction zone formed within the Austroalpine continental crust at the site of a Permian rift.
- (3) The segment of the EGU is part of the distal Permian rift zone, which finally led to the opening of the Meliata Ocean during Middle Triassic times. The stretched continental crust was subducted to mantle depth and then rapidly exhumed by upward motion due to buoyancy during early Late Cretaceous times.
- (4) We propose a new model of accretion of lower Middle/Lower Central Austroalpine and Lower Austroalpine units by continuous downward motion of the Meliata oceanic slab.

Supplementary information

Supplementary information accompanies this paper at <https://doi.org/10.1186/s00015-020-00369-z>.

Additional file 1: Table S1. U-Pb analytical data.

Additional file 2: Table S2. REE contents of zircon spots.

Additional file 3: Table S3. Zirconium saturation thermometer.

Acknowledgements

We acknowledge detailed, careful and constructive comments by journal reviewers, Cees-Jan de Hoog and Marian Janák, and by the guest editor Othmar Müntener. Deep thanks to Dr. Chao Zhang from Shandong University of Technology for his help during the field investigation. We thank the staff of Beijing Createch Testing Technology Co. Ltd. for their technical support during zircon U–Pb dating and constructive comments leading to improvement of the manuscript. We thank the colleagues from Jilin University and Key Lab of Submarine Geoscience and Prospecting Techniques of Ocean University of China.

Authors' contributions

FN, YL, RC (as part of her PhD thesis) and JG designed the study. Samples were collected together with JG, RC, SY and WJ. Analytical work and first data assessment was mostly done by RC, QG, QH and WL. All authors contributed to the interpretation of data and writing of the paper under the lead of RC. JG peculiarly contributed subchapter 6.4. All authors read and approved the final manuscript.

Funding

This study was financially supported by the National Natural Science Foundation of China (Grant No. 91755212), Taishan Scholars (ts20190918) and Qingdao Leading innovation talents (no. 19-3-2-19-zhc) to Yongjiang Liu and by a PhD grant of the State Scholarship Fund from CSC (201906170046) to Ruihong Chang.

Availability of data and materials

The entire new data set is included in the paper.

Ethics approval and consent to participate

Not applicable.

Consent for publication

Not applicable.

Competing interests

The authors declare that they have no competing interests.

Author details

¹ Department of Geography and Geology, University of Salzburg, 5020 Salzburg, Austria. ² Key Lab of Submarine Geoscience and Prospecting Techniques, Frontiers Science Center for Deep Ocean Multispheres and Earth System, MOE, College of Marine Geosciences, Ocean University of China, Qingdao 266100, China. ³ Laboratory for Marine Mineral Resources, Qingdao National Laboratory for Marine Science and Technology, Qingdao 266237, China. ⁴ College of Earth Science, Institute of Disaster Prevention, Sanhe 065201, Hebei, China. ⁵ College of Earth Sciences, Jilin University, Changchun 13006, Jilin, People's Republic of China.

Received: 18 April 2020 Accepted: 25 August 2020

Published online: 02 October 2020

References

- Boehnke, P., Watson, E. B., Trail, D., Harrison, T. M., & Schmitt, A. K. (2013). Zircon saturation revisited. *Chemical Geology*, *351*, 324–334.
- Bonin, B. (2007). A-type granites and related rocks: evolution of a concept, problems and prospects. *Lithos*, *97*(1), 1–29.
- Bouvier, A., Vervoort, J. D., & Patchett, P. J. (2008). The Lu–Hf and Sm–Nd isotopic composition of CHUR, constraints from unequilibrated chondrites and implications for the bulk composition of terrestrial planets. *Earth and Planetary Science Letters*, *273*, 48–57.
- Boynton, W. V. (1984). Geochemistry of the rare earth elements: meteorite studies. In P. Henderson (Ed.), *Rare earth element geochemistry* (pp. 63–114). Amsterdam: Elsevier.
- Braud, E., Stüwe, K., & Proyer, A. (2010). Pseudosection modelling for a selected eclogite body from the Koralpe (Hohl), Eastern Alps. *Mineralogy and Petrology*, *99*, 75–87.
- Channell, J. E. T., & Kozur, H. W. (1997). How many oceans? Meliata, Vardar and Pindos oceans in Mesozoic Alpine paleogeography. *Geology*, *25*(2), 183–186.
- Clerc, C., Jolivet, L., & Ringenbach, J.-C. (2015). Ductile extensional shear zones in the lower crust of a passive margin. *Earth and Planetary Science Letters*, *431*, 1–7.
- Cohen, K. M., Finney, S. C., Gibbard, P. L., & Fan, J.-X. (2013). The ICS International Chronostratigraphic Chart. *Episodes*, *36*(3), 199–204.
- Corfu, F., Hanchar, J. M., Hoskin, P. W. O., & Kinny, P. (2003). Atlas of zircon textures. *Reviews in Mineralogy and Geochemistry*, *53*, 469–500.
- Dallmeyer, R. D., Handler, R., Neubauer, F., & Fritz, H. (1998). Sequence of thrusting within a thick-skinned tectonic wedge: evidence from ⁴⁰Ar/³⁹Ar ages from the Austroalpine nappe complex of the Eastern Alps. *Journal of Geology*, *106*, 71–86.
- De Hoog, J. C. M., Janák, M., Vrabec, M., & Froitzheim, N. (2009). Serpentinised peridotites from an ultrahigh-pressure terrane in the Pohorje Mts. (Eastern Alps, Slovenia): geochemical constraints on petrogenesis and tectonic setting. *Lithos*, *109*(3–4), 209–222.
- De Hoog, J. C. M., Janák, M., Vrabec, M., & Hattori, K. H. (2011). Ultramafic cumulates of oceanic affinity in an intracontinental subduction zone: ultrahigh-pressure garnet peridotites from pohorje (Eastern Alps, Slovenia). In L. F. Dobrzhinetskaya, S. W. Faryad, S. Wallis, & S. Cuthbert (Eds.), *Ultra-high-pressure metamorphism, 25 years after the discovery of coesite and diamond* (pp. 399–439). Amsterdam: Elsevier.
- Debon, F., & Le Fort, P. A. (1983). Chemical–mineralogical classification of common plutonic rocks and associations. *Transactions of the Royal Society of Edinburgh Earth and Environmental Science*, *73*(3), 135–149.
- Eby, G. N. (1990). The A-type granitoids: a review of their occurrence and chemical characteristics and speculations on their petrogenesis. *Lithos*, *26*(1), 115–134.
- Eby, G. N. (1992). Chemical subdivision of the A-type granitoids: petrogenetic and tectonic implications. *Geology*, *20*, 641–644.
- Fodor, L. I., Gerdes, A., & Dunkl, I. (2008). Miocene emplacement and rapid cooling of the Pohorje pluton at the Alpine-Pannonian-Dinaridic junction, Slovenia. *Swiss Journal of Geosciences*, *101*(1), 255–271.
- Frost, B. R., Barnes, C. G., Collins, W. J., Arculus, R. J., Ellis, D. J., & Frost, C. D. (2001). A geochemical classification for granitic rocks. *Journal of Petrology*, *42*(11), 2033–2048.

- Froitzheim, N., Pleuger, J., Roller, S., & Nagel, T. (2003). Exhumation of high- and ultrahigh-pressure metamorphic rocks by slab extraction. *Geology*, *31*, 925–928.
- Froitzheim, N., Plašienka, D., & Schuster, R. (2008). Alpine tectonics of the Alps and Western Carpathians. In T. McCann (Ed.), *The Geology of Central Europe. Mesozoic and Cenozoic* (Vol. 2, pp. 1141–1232). London: Geological Society of London.
- Griffin, W. L., Wang, X., Jackson, S. E., Pearson, N. J., O'Reilly, S. Y., Xu, X. S., Zhou, Z. M. (2002). Zircon chemistry and magma mixing, SE China, in-situ analysis of Hf isotopes, Tonglu and Pingtan igneous complexes. *Lithos*, *61*, 237–269.
- Grimes, C. B., John, B. E., Kelemen, P. B., Mazdab, F. K., Wooden, J. L., Cheadle, M. J., Hanghøj, K., & Schwartz, J. J. (2007). Trace element chemistry of zircons from oceanic crust: a method for distinguishing detrital zircon provenance. *Geology*, *35*, 643–646.
- Habler, G., & Thöni, M. (1998). New petrological and structural data from the eclogite bearing polymetamorphic eastern Austroalpine basement nappes (NW Saualpe, Austria). *Forschungsh. C*, *471*, 86–88.
- Habler, G., Thöni, M., & Miller, C. (2007). Major and trace element chemistry and Sm–Nd age correlation of magmatic pegmatite garnet overprinted by eclogite-facies metamorphism. *Chemical Geology*, *241*, 4–22.
- Habler, G., & Thöni, M. (2001). Preservation of Permo-Triassic low-pressure assemblages in the Cretaceous high-pressure metamorphic Saualpe crystalline basement (Eastern Alps, Austria). *Journal of Metamorphic Geology*, *19*(6), 679–697.
- Hastie, A. R., Kerr, A. C., Pearce, J. A., & Mitchell, S. F. (2007). Classification of altered volcanic island arc rocks using immobile trace elements: development of the Th–Co discrimination diagram. *Journal of Petrology*, *48*(12), 2341–2357.
- Hauzenberger, C. A., Taferner, H., & Konzett, J. (2016). Genesis of chromium-rich kyanite in eclogite-facies Cr-spinel-bearing gabbroic cumulates, Pohorje Massif, Eastern Alps. *American Mineralogist*, *101*(2), 448–460.
- Herg, A., & Stüwe, K. (2018). Tectonic interpretation of the metamorphic field gradient south of the Koralpe in the Eastern Alps. *Austrian Journal of Earth Sciences*, *111*(2), 155–170.
- Hoskin, P. W. O., & Schaltegger, U. (2003). The composition of zircon and igneous and metamorphic petrogenesis. *Reviews of Mineralogy and Geochemistry*, *53*, 27–62.
- Hou, K. J., Li, Y. H., & Tian, Y. Y. (2009). In situ U–Pb zircon dating using laser ablation-multi ion counting-ICP-MS. *Mineral Deposits*, *28*(4), 481–492. **(in Chinese with English abstract)**.
- Hou, K. J., Yanhe, L. I., & Xie, G. Q. (2007). Laser ablation-MC-ICP-MS technique for Hf isotope microanalysis of zircon and its geological applications. *Acta Petrologica Sinica*, *23*, 2595–2604.
- Jackson, S. E., Pearson, N. J., Griffin, W. L., & Belousova, E. A. (2004). The application of laser ablation-inductively coupled plasma-mass spectrometry to in situ U–Pb zircon geochronology. *Chemical Geology*, *211*, 47–69.
- Janák, M., Cornell, D., Froitzheim, N., De Hoog, J. C. M., Broska, I., Vrabec, M., et al. (2009). Eclogite-hosting metapelites from the Pohorje Mountains (Eastern Alps): P–T evolution, zircon geochronology and tectonic implications. *European Journal of Mineralogy*, *21*, 1191–1212.
- Janák, M., Froitzheim, N., Lupták, B., Vrabec, M., & Krogh Ravná, E. J. (2004). *First evidence for ultrahigh-pressure metamorphism of eclogites in Pohorje. Tracing deep continental subduction in the Eastern Alps*. Slovenia: Tectonics. <https://doi.org/10.1029/2004tc001641>.
- Janák, M., Froitzheim, N., Vrabec, M., Krogh, Ravná, E. J., & De Hoog, J. C. M. (2006). Ultrahigh-pressure metamorphism and exhumation of garnet peridotite in Pohorje, Eastern Alps. *Journal of Metamorphic Geology*, *24*, 19–31.
- Janák, M., Froitzheim, N., Yoshida, K., Sasinková, V., Nosko, M., Kobayashi, T., et al. (2015). Diamond in metasedimentary crustal rocks from Pohorje, Eastern Alps: a window to deep continental subduction. *Journal of Metamorphic Geology*, *33*, 495–512.
- Jochum, K. P., Willbold, M., Raczek, I., Stoll, B., & Herwig, K. (2005). Chemical characterisation of the usgs reference glasses GSA-1G, GSC-1G, GSD-1G, GSE-1G, BCR-2G, BHVO-2G and BIR-1G using EPMA, ID-TIMS, ID-ICP-MS and LA-ICP-MS. *Geostandards and Geoanalytical Research*, *29*(3), 285–302.
- King, P. L., White, A. J. R., Chappell, B. W., & Allen, C. M. (1997). Characterization and origin of aluminous A-type granites from the Lachlan Fold Belt, southeastern Australia. *Journal of Petrology*, *38*, 371–391.
- Kirst, F., Sandmann, S., Nagel, T. J., Froitzheim, N. N., & Janák, M. (2010). Tectonic evolution of the southeastern part of the Pohorje Mountains (Eastern Alps, Slovenia). *Geologica Carpathica*, *61*, 451–461.
- Knoll, T., Schuster, R., Huet, B., Mai, H., Onuk, P., Horschinegg, M., et al. (2018). Spodumene pegmatites and related leucogranites from the austroalpine unit (Eastern Alps, Central Europe): field relations, petrography, geochemistry, and geochronology. *The Canadian Mineralogist*, *56*(4), 489–528.
- Kozur, H. (1991). The evolution of the Meliata-Hallstatt ocean and its significance for the early evolution of the Eastern Alps and Western Carpathians. *Palaeogeography, Palaeoclimatology, Palaeoecology*, *87*, 109–135.
- Kunz, B., Manzotti, P., von Niederhäusern, B., Engi, M., Giuntoli, F., & Lanari, P. (2018). Permian high temperature metamorphism in the Western Alps (NW Italy). *International Journal of Earth Sciences*, *107*, 203–229.
- Kurz, W., Fritz, H., Tenczer, V., & Unzog, W. (2002). Tectonometamorphic evolution of the Koralm Complex (Eastern Alps): constraints from microstructures and textures of the 'Plattengneis' shear zone. *Journal of Structural Geology*, *24*(12), 1957–1970.
- Lein, R. (1987). Evolution of the Northern Calcareous Alps during Triassic times. In H. W. Flügel & P. Faupl (Eds.), *Geodynamics of the Eastern Alps* (pp. 85–102). Wien: Deuticke.
- Liu, Y. S., Gao, S., Hu, Z. C., Gao, C. G., Zong, K. Q., & Wang, D. B. (2010). Continental and oceanic crust recycling-induced melt-peridotite interactions in the Trans-North China Orogen: U–Pb dating, Hf isotopes and trace elements in zircons from mantle xenoliths. *Journal of Petrology*, *51*, 537–571.
- Liu, Y., Genser, J., Handler, R., Friedl, G., & Neubauer, F. (2001). ⁴⁰Ar/³⁹Ar muscovite ages from the Penninic/Austroalpine plate boundary, Eastern Alps. *Tectonics*, *20*, 528–547.
- Ludwig, K. R. (2003). Isoplot 3.00: a geochronological toolkit for Microsoft Excel. *Berkeley Geochronology Center Special Publication*, *4*, 1–70.
- Manzotti, P., Rubatto, D., Zucali, M., El Korh, A., Cenki-Tok, B., Ballèvre, M., et al. (2018). Permian magmatism and metamorphism in the Dent Blanche nappe: constraints from field observations and geochronology. *Swiss Journal of Geosciences*, *111*, 79–97.
- McDonough, W. F., & Sun, S. S. (1995). The composition of the Earth. *Chemical Geology*, *120*(3–4), 223–253.
- Middlemost, E. A. K. (1994). Naming materials in the magma/igneous rock system. *Earth-Science Reviews*, *37*, 215–224.
- Miller, C. (1990). Petrology of the type locality eclogites from the Koralpe and Saualpe (Eastern Alps). *Austria. Schweizerische mineralogische und petrographische Mitteilungen*, *70*(2), 287–300.
- Miller, C. F., McDowell, S. M., & Mapes, R. W. (2003). Hot and cold granites? Implications of zircon saturation temperatures and preservation of inheritance. *Geology*, *31*, 529–532.
- Miller, C., Mundil, R., Thöni, M., & Konzett, J. (2005a). Refining the timing of eclogite metamorphism: a geochemical, petrological, Sm–Nd and U–Pb case study from the Pohorje Mountains, Slovenia (Eastern Alps). *Contributions of Mineralogy and Petrology*, *150*, 70–84.
- Miller, C., Thöni, M., Konzett, J., Kurz, W., & Schuster, R. (2005b). Eclogites from the Koralpe and Saualpe type-localities, eastern Alps, Austria. *Mitteilungen der Österreichischen Mineralogischen Gesellschaft*, *150*, 227–263.
- Miller, C., Zanetti, A., Thöni, M., & Konzett, J. (2007). Eclogitisation of gabbroic rocks: redistribution of trace elements and Zr in rutile thermometry in an Eo-Alpine subduction zone (Eastern Alps). *Chemical Geology*, *239*(1–2), 96–123.
- Mioč, P., & Žnidarčič, M. (1977). *Geological map of SFRJ 1:100 000*. Federal Geological Survey of Yugoslavia, Beograd: Sheet Slovenj Gradec.
- Morauf, W. (1980). Die permische Differentiation und die alpidische Metamorphose des Granitgneises von Rb (Koralpe) mit Rb–Sr- und K–Ar-Isotopenbestimmung. *Tschermaks Mineralogische und Petrographische Mitteilungen*, *27*, 169–185.
- Morel, M. L. A., Nebel, O., Nebel-Jacobsen, Y. J., Miller, J. S., & Vroon, P. Z. (2008). Hafnium isotope characterization of the GJ-1 zircon reference material by solution and laser-ablation MC-ICPMS. *Chemical Geology*, *255*(1–2), 231–235.
- Neubauer, F. (1994). Comment to M. Wägrich, "Subcrustal tectonic erosion in orogenic belts A model for the Late Cretaceous subsidence of the Northern Calcareous Alps (Austria)". *Geology*, *22*, 855–856.
- Neubauer, F., Dallmeyer, R. D., Dunkl, I., & Schirnik, D. (1995). Late Cretaceous exhumation of the metamorphic Gleinalm dome, Eastern Alps:

- kinematics, cooling history and sedimentary response in a sinistral wrench corridor. *Tectonophysics*, 242, 79–89.
- Neubauer, F., Genser, J., & Handler, R. (2000). The Eastern Alps: result of a two-stage collision process. *Mitteilungen der Österreichischen Geologischen Gesellschaft*, 92, 117–134.
- Passchier, C. W., & Trouw, R. A. J. (2005). *Microtectonics*. Berlin: Springer Science & Business Media.
- Peccerillo, A., & Taylor, S. R. (1976). Geochemistry of Eocene calc-alkaline volcanic rocks from the Kastamonu area, northern Turkey. *Contributions to Mineralogy and Petrology*, 58(1), 63–81.
- Plašienka, D. (2018). Continuity and episodicity in the early Alpine tectonic evolution of the Western Carpathians: how large-scale processes are expressed by the orogenic architecture and rock record data. *Tectonics*. <https://doi.org/10.1029/2017TC004779>.
- Putiš, M., Li, X.-H., Yang, Y.-H., Kl, Q. L., Nemeč, O., Ling, X.-X., et al. (2018). Permian pyroxenite dykes in harzburgite with signatures of the mantle, subduction channel and accretionary wedge evolution (Austroalpine Unit, Eastern Alps). *Lithos*, 314, 165–186.
- Ratschbacher, L., Frisch, W., & Linzer, H. G. (1991). Lateral extrusion in the Eastern Alps, part 2: structural analysis. *Tectonics*, 10(2), 257–271.
- Ratschbacher, L., Frisch, W., Neubauer, F., Schmid, S. M., & Neugebauer, J. (1989). Extension in compressional orogenic belts: the eastern Alps. *Geology*, 17(5), 404–407.
- Rubatto, D. (2002). Zircon trace element geochemistry: distribution coefficients and the link between U-Pb ages and metamorphism. *Chemical Geology*, 184, 123–138.
- Rubatto, D. (2017). Zircon: the Metamorphic Mineral. *Reviews in Mineralogy and Geochemistry*, 83, 261–295.
- Sandmann, S., Herwartz, D., Kirst, F., Froitzheim, N., Nagel, T. J., Fonseca, R. O. C., et al. (2016). Timing of eclogite-facies metamorphism of mafic and ultramafic rocks from the Pohorje Mountains (Eastern Alps, Slovenia) based on Lu–Hf garnet geochronometry. *Lithos*, 262, 576–585.
- Sassi, R., Mazzoli, C., Miller, C., & Konzett, J. (2004). Geochemistry and metamorphic evolution of the Pohorje Mountain eclogites from the easternmost Austroalpine basement of the Eastern Alps (Northern Slovenia). *Lithos*, 78(3), 235–261.
- Schaffhauser, M., Krainer, K., & Sanders, D. (2015). Early Permian carbonate shelf margin deposits: the type section of the Troglkofel Formation (Artinskian/Kungurian), Carnic Alps. *Austria/Italy. Austrian Journal of Earth Sciences*, 108(2), 277–301.
- Schaltegger, U., & Brack, P. (2007). Crustal-scale magmatic systems during intracontinental strike-slip tectonics: U, Pb and Hf isotopic constraints from Permian magmatic rocks of the Southern Alps. *International Journal of Earth Sciences (Geologische Rundschau)*, 96, 1131–1151.
- Schmid, S. M., Fügenschuh, B., Kissling, E., & Schuster, R. (2004). Tectonic map and overall architecture of the Alpine orogeny. *Eclogae Geologicae Helveticae*, 97, 93–117.
- Schorn, S. (2018). Dehydration of metapelites during high-P metamorphism: the coupling between fluid sources and fluid sinks. *Journal of Metamorphic Geology*, 36(3), 369–391.
- Schorn, S., & Stüwe, K. (2016). The Plankogel detachment of the Eastern Alps: petrological evidence for an orogen-scale extraction fault. *Journal of Metamorphic Geology*, 34(2), 147–166.
- Schulz, B. (2017). Polymetamorphism in garnet micaschists of the Saualpe Eclogite Unit (Eastern Alps, Austria), resolved by automated SEM methods and EMP–Th–U–Pb monazite dating. *Journal of Metamorphic Geology*, 35(2), 141–163.
- Schuster, R., & Stüwe, K. (2008). Permian metamorphic event in the Alps. *Geology*, 36, 603–606.
- Schuster, R., Tropper, P., Krenn, E., Finger, F., Frank, W., & Philippitsch, R. (2015). Prograde Permo-Triassic metamorphic HT/LP assemblages from the Austroalpine Jenig Complex (Carinthia, Austria). *Austrian Journal of Earth Sciences*, 108(1), 73–90.
- Soderlund, U., Patchett, P. J., Vervoort, J. D., & Isachsen, C. E. (2004). The ¹⁷⁶Lu decay constant determined by Lu–Hf and U–Pb isotope systematics of Precambrian mafic intrusions. *Earth and Planetary Science Letters*, 219, 311–324.
- Stipp, M., Stünitz, H., & Heilbronner, R. (2002a). The eastern Tonale fault zone: a 'natural laboratory' for crystal plastic deformation of quartz over a temperature range from 250 to 700 C. *Journal of Structural Geology*, 24(12), 1861–1884.
- Stipp, M., Stünitz, H., & Heilbronner, R. (2002b). Dynamic recrystallization of quartz: correlation between natural and experimental conditions. *Geological Society, London, Special Publications*, 200(1), 171–190.
- Stipp, M., Tullis, J., & Scherwath, M. (2010). A new perspective on paleo-epizometry: dynamically recrystallized grain size distributions indicate mechanism changes. *Geology*, 38(8), 759–762.
- Stüwe, K., & Schuster, R. (2010). Initiation of subduction in the Alps: continent or ocean? *Geology*, 38, 175–178.
- Sun, S. S., & McDonough, W. F. (1989). Chemical and isotopic systematics of oceanic basalts: implications for mantle composition and processes. *Geological Society, London, Special Publications*, 42(1), 313–345.
- Taylor, S. R., & McLennan, S. M. (1985). *The continental crust: Its composition and evolution* (p. 328). London: Blackwell Scientific.
- Thöni, M. (2002). Sm–Nd isotope systematics in garnet from different lithologies Eastern Alps age results, and an evaluation of potential problems for garnet Sm–Nd chronometry. *Chemical Geology*, 2003, 194(4), 353–379.
- Thöni, M. (2006). Dating eclogite-facies metamorphism in the Eastern Alps—approaches, results, interpretations: a review. *Mineralogy and Petrology*, 88(1–2), 123–148.
- Thöni, M., & Jagoutz, E. (1992). Some new aspects of dating eclogites in orogenic belts: sm–Nd, Rb–Sr, and Pb–Pb isotopic results from the Austroalpine Saualpe and Koralpe type-locality (Carinthia/Styria, southeastern Austria). *Geochimica et Cosmochimica Acta*, 56, 347–368.
- Thöni, M., & Miller, C. (2000). Permo-Triassic pegmatites in the eo-Alpine eclogite-facies Koralpe complex, Austria: age and magma source constraints from mineral chemical, Rb–Sr and Sm–Nd isotope data. *Schweizerische Mineralogische und Petrographische Mitteilungen*, 80(2), 169–186.
- Thöni, M., & Miller, C. (2009). The "Permian event" in the Eastern European Alps: sm–Nd and P–T data recorded by multi-stage garnet from the Plankogel unit. *Chemical Geology*, 260, 20–36.
- Thöni, M., & Miller, C. (2010). Andalusite formation in a fast exhuming high-P wedge: textural, microchemical, and Sm–Nd and Rb–Sr age constraints for a Cretaceous PTt path at Kienberg, Saualpe (Eastern Alps). *Austrian Journal of Earth Sciences*, 103(2), 118–131.
- Thöni, M., Miller, C., Blicher-Toft, J., Whitehouse, M. J., Konzett, J., & Zanetti, A. (2008a). Timing of high-pressure metamorphism and exhumation of the eclogite type-locality (Kupplerbrunn–Prickler Halt, Saualpe, southeastern Austria): constraints from correlations of the Sm–Nd, Lu–Hf, U–Pb and Rb–Sr isotopic systems. *Journal of Metamorphic Geology*, 26(5), 561–581.
- Thöni, M., Miller, C., Zanetti, A., Habler, G., & Goessler, W. (2008b). Sm–Nd isotope systematics of high-REE accessory minerals and major phases: iD-TIMS, LA-ICP-MS and EPMA data constrain multiple Permian-Triassic pegmatite emplacement in the Koralpe, Eastern Alps. *Chemical Geology*, 254, 216–237.
- Tropper, P., Harlov, D., Krenn, E., Finger, F., Rhede, D., & Bernhard, F. (2007). Zr-bearing minerals as indicators for the polymetamorphic evolution of the eastern, lower Austroalpine nappes (Stubenberg Granite contact aureole, Styria, Eastern Alps, Austria). *Lithos*, 95, 72–86.
- Villaseca, C., Barbero, L., & Herreros, V. (1998). A re-examination of the typology of peraluminous granite types in intracontinental orogenic belts. *Earth and Environmental Science Transactions of The Royal Society of Edinburgh*, 89(2), 113–119.
- Vrabec, M., Janák, M., Froitzheim, N., & de Hoog, J. C. M. (2012). Phase relations during peak metamorphism and decompression of the UHP kyanite eclogites, Pohorje Mountains (Eastern Alps, Slovenia). *Lithos*, 144, 40–55.
- Vrabec, M., Rogan Šmuc, N., & Vrabec, M. (2018). Calcite deformation twins in Pohorje marbles. *Geologija*, 61(1), 73–84.
- Watson, E. B., & Harrison, T. M. (1983). Zircon saturation revisited: temperature and composition effects in a variety of crustal magma types. *Earth and Planetary Science Letters*, 64, 295–304.
- Whalen, J. B., Currie, K. L., & Chappell, B. W. (1987). A-type granites: geochemical characteristics, discrimination and petrogenesis. *Contributions to Mineralogy and Petrology*, 95(4), 407–419.
- Wiesinger, M., Neubauer, F., & Handler, R. (2006). Exhumation of the Saualpe eclogite unit, Eastern Alps: constraints from ⁴⁰Ar/³⁹Ar ages. *Mineralogy and Petrology*, 88, 149–180.

Winchester, J. A., & Floyd, P. A. (1977). Geochemical discrimination of different magma series and their differentiation products using immobile elements. *Chemical Geology*, 20, 325–343.

Žnidarčič M. & Mioč P. (1989). *Geological map of SFRJ 1:100.000, Sheet Maribor*. Federal Geological Survey of Yugoslavia, Beograd.

Publisher's Note

Springer Nature remains neutral with regard to jurisdictional claims in published maps and institutional affiliations.

Submit your manuscript to a SpringerOpen[®] journal and benefit from:

- ▶ Convenient online submission
- ▶ Rigorous peer review
- ▶ Open access: articles freely available online
- ▶ High visibility within the field
- ▶ Retaining the copyright to your article

Submit your next manuscript at ▶ [springeropen.com](https://www.springeropen.com)
